FRICTIONAL DAMPER TO ENHANCE DYNAMIC STABILITY IN ENDMILLING

By

M-CHARLES-V STANISLAUS

A THESIS PRESENTED TO THE GRADUATE SCHOOL
OF THE UNIVERSITY OF FLORIDA IN PARTIAL FULFILLMENT
OF THE REQUIREMENTS FOR THE DEGREE OF
MASTER OF SCIENCE

UNIVERSITY OF FLORIDA

2003

ACKNOWLEDGMENTS

The author wishes to express his gratitude to Dr. John Ziegert for being the advisor and the person responsible for the completing the research successfully.

The author would like to express his sincere thanks to Dr. John Schueller, who gave him the opportunity to join the Machine Tool Research Center (MTRC) and was always ready to help him when needed.

The author would like to specially thank Dr. Tony Schmitz for providing guidance and support to complete the experiments.

The author also wishes to extend his gratitude to Dr. Brian Mann for his valuable suggestions during the research and all the members of the MTRC for their friendship, criticism and assistance.

Finally the author is grateful to his family and friends for their moral support, without which this task could not be accomplished.

TABLE OF CONTENTS

APPENDIX

LIST OF FIGURES

Abstract of Thesis Presented to the Graduate School
of the University of Florida in Partial Fulfillment of the
Requirements for the Degree of Master of Science

FRICTIONAL DAMPER TO ENHANCE DYNAMIC STABILITY IN ENDMILLING

By

M-Charles-V Stanislaus

December 2003

Chair: John C. Ziegert
Major Department: Mechanical and Aerospace Engineering

Chatter in milling is considered to be one of the biggest problems in the machining manufacturing process. Machine tools capable of cutting materials with impressive speeds and feed rates are often constrained to perform below their capacity because of stability limits on the milling process. However, intensive research has focused on the design of tools that increase milling stability leading to higher material removal rates.

The research presented in this thesis implements a frictional damper to improve the stability of cutting tools during the milling process, particularly endmills. Theoretical models were developed and the magnitude of frictional work produced by the damper was obtained by optimizing the physical dimensions of the design. Three different tools, solid, hollow, and damped, were selected for investigation and were fabricated with identical profiles. Initial tests to understand the tool characteristics were performed by measuring the frequency response function (FRF) of the tools.

The effect of spindle speeds on the dynamic behavior of the spindle/holder/tool at the tool point was studied by obtaining the rotating FRF at different speeds. Stability

lobes were obtained based on the measurements and the difference in stability limits between the static and rotating FRF measurements was plotted. The effect of the damper on the cutting tool dynamics, compared with the solid and the hollow tools, was also determined based on measured FRFs at the tool point.

To verify the preliminary results, a series of cutting tests were performed on the three tools, and a method to identify the stability limits was developed by recording the audio signal during the cut. The results were then plotted to show the effect of spindle speed on stability limits providing a measure of performance of the three tools.

The concept of frictional damping was verified when the damped tool achieved a sixty-six percent improvement in cutting depth over the solid tool. The results also showed that lobes developed from dynamic measurements are more realistic than statically generated, non-rotating FRFs.

CHAPTER 1
INTRODUCTION

The demand for increase in productivity, with good surface finish and better tool life, continually pushes manufacturing industries to find optimal combinations of machines and cutting tools. Extensive research in structural dynamics and high-speed machining has helped us more clearly understand, the interactions between spindle, tool and work piece.

In past years, aluminum parts of thin cross-sections used in aerospace industries were made from formed sheet metal assembled together. This made a huge impact on the overall cost of manufacturing aircraft components by increasing the assembly cost and weight on the finished product. With the advent of high-speed machining, mechanical and aerospace designers made monolithic parts from a stock of material and were able to reduce the overall cost of production. It was quite impressive to note that they were able to reduce the production time by 50% [1]. In order to reduce production time, it is expected that the machine tools are required to have a high-speed and feed rate. For over a decade this has been motivating researchers, to improve the performance of machine tool and cutters to increase the material removal rate (MRR). In the area of structural dynamics, research activities on modifying cutting tools to increase their stiffness and damping have been quite successful.

In an effort to achieve a similar objective, this research work involves designing, analyzing and implementing a damper to improve the stability of end mills and to achieve higher material removal rate.

Long end-mills, the most widely used tool in high-speed machining operations, undergo a bending vibration similar to a cantilevered structure during machining. Beyond a certain depth, the vibrations may become unstable. This characteristic of the tool creates an uneven surface, reducing the tool life and hence results in low material removal rate. The term often associated with this phenomenon is called chatter.

Chatter is most commonly explained as a self-excited vibration that occurs due to regeneration of waviness. The relative vibrations between the tool and the work piece causes a wavy surface to be generated. Subsequent teeth encounter this wavy surface, which produces chips of varying thickness [2]. The chip thickness variation causes a periodic variation in the cutting force, which in certain conditions can lead to larger amplitude vibrations, or chatter.

It is known that the limiting stable depth of cut for a given tool is limited by the dynamic stiffness of the most flexible mode of vibration. The dynamic stiffness is dependent on both the modal stiffness and the damping of the system. Therefore, if a tool can be designed with increased damping, it should offer enhanced stability against chatter.

Numerous researchers such as Edhi and Hoshi [3], Slocum [4], and Schmitz and Donaldson [5] have investigated damping in vibrating structures and have suggested various techniques to increase damping. Some of the previous work related to this area will be presented briefly in the next chapter. A description of the intended damper design and a mathematical model used to predict energy dissipation and to obtain the design parameters will be presented in Chapter 3. Chapter 4 will discuss the instrumentation used to understand the tool characteristics. Also a brief description of various fixtures and

tooling necessary to get the measurements from the test will be given. A method to obtain the frequency response functions (FRFs) at different spindle speeds will be explained in detail. The experimental design to test the damper and the results from the cutting tests will be discussed in Chapter 5. Also, a method to identify the chatter frequencies during machining will be presented along with plots to compare the sound magnitudes of stable and unstable cuts. Finally, the results obtained from the cutting tests will be discussed to provide conclusions and recommendations for future work.

CHAPTER 2
LITERATURE STUDY ON VIBRATION CONTROL

Self-excited vibration in cutting tools has been a significant problem in the area of high-speed machining due to its detrimental effect on the tool and the machined surface. This chapter reviews some of the research work done to increase the stability of vibrating structures; particularly, chatter control on cutting tools.

In an effort to control vibration in cutting tools, Edhi and Hoshi [3] developed a method to stabilize the high frequency chatter vibration in boring bars by employing a friction damper. They observed that boring bars during machining, when unstable, produced chatter frequency of more than 1 KHz. This caused a reduced tool life and a bad surface quality on the machined surface. In order to improve the tool life and to reduce chatter, they implemented a frictional damper. This damper was characterized by a simple structure of a mass attached to the vibrating boring bar with a piece of permanent magnet. The principle behind introducing this type of damper was that Coulomb and viscous friction dissipates the energy produced due to vibrations at the interface between the vibrating tool and the damper (mass). They observed that the results were impressive when they performed the cutting test on the tool with the damper on it; the damper needed no tuning and was effective in eliminating high frequency chatter.

Schmitz and Donaldson [5] established a method that studied the interaction between the tool, holder, and the spindle and introduced a coupling factor that can be used to predict the critical depth of cut on stability lobe graphs. His work, based on the

concept of receptance coupling, analyzed the individual FRFs (frequency response function) of the tool, holder, and the spindle and by analytical method developed a model that predicted the dynamic response of the final assembly. This method can be used to analytically predict and achieve the optimal overhang for maximum stability. By varying the lengths of the tool over-hang, Schmitz found out that there were interactions between the tool and the spindle modes and this affected the magnitude of the frequency response of the final assembly. This idea of tool tuning was also used to a certain extent in the current research work.

Efforts to investigate the problems due to chatter have also been carried out at the Machine Tool Research Center in past years. Cobb [6] used a tuned damper to control the chatter in boring bars. He developed two types of damper, one with end caps and mass sandwiched between them and the other, where a mass is slit half and bolted together. In both these types, the mass was mounted on to the boring bar. The idea behind this was, when the boring bar vibrates, the mass attached to it, in turn vibrates out of phase and by the shear force produced at the interface, provided the damping effect. This idea was very successful at the frequencies to which the mass was tuned.

Smith [7], Keyvanmanesh [8], and Cheng [9] at MTRC did an extensive research in understanding the dynamic characteristics of the tool and spindle to control chatter during machining.

Keyvanmanesh [8] developed an algorithm to detect the chatter region based on the information obtained from the cutting tests on different end mills. Similar to the work done by Smith, he did a time domain simulation using the values obtained from the

dynamic response of the tool to plot the stability lobes. By using the control system developed from the algorithm, he was able to locate the stable speed more clearly.

A tool in its holder is very similar to a cantilevered beam. Research on structural damping has given a great knowledge in understanding the behavior of a tool. Cook et al. [10] at the University of Florida, developed damping mechanisms to control vibrations on traffic signal structures. Traffic signal structures that are subjected to cyclic loading due to the wind and fast moving vehicles, sometimes, result in premature fatigue failures. They investigated this problem and proposed devices to provide damping to the structures. Some of them include tuned mass dampers, liquid dampers, friction dampers, and impact dampers. It was later found after testing, that impact dampers served better in controlling the vibrations. The types of impact dampers used were a spring/mass liquid impact damper and a tapered impact damper. The spring mass liquid impact damper, which they devised, consisted of a mass vertically supported inside a steel pipe. When the mast arm moved, the mass impacted the plate enclosing the steel pipe and disrupted the movement of the mast. The liquid filled inside acted like a pool and formed a thin film between the mass and the sidewalls of the pipe thus making the damper a combination of friction and impact device. The tapered impact damper, acted similar to the mass impact damper except that the steel pipe is tapered at the region of impact and provided both horizontal and vertical damping.

The basic idea from which the current research damper model was based on was the work done by Slocum on damping bending in beams. In his book, Slocum [4] introduced the concept of friction damping between layered elements. The book explains that, when two cantilevered beams stacked on top of each other undergo bending there

occurs a relative shear motion between the inner surfaces of the layered elements causing friction energy to be produced at the interface, which in turn, used to reduce the deflection of the layered beam. One of his patented works [11] implements this idea. He developed a method to damp bending vibrations in beams and similar structures. He made a hollow beam and inserted one or more structural members along its approximate length and filled in the annulus between the inner and out member with a viscoelastic energy absorbing material. When the beams were bending, it resulted in a relative shear displacement between the beams thereby shearing the viscoelastic material and dissipating the energy produced. He also derived equations to calculate the relative displacement between the layered elements.

With this idea, a damper model will be designed and developed. As the research is being done on a work already started at the MTRC, analytical models of various proposed designs will be presented along with the results to choose the right model for the research. The basic idea behind all the proposed designs is to provide centrifugal damping effect to the cutting tools.

CHAPTER 3
ANALYTICAL AND FINITE ELEMENT MODEL OF THE DAMPER

Two theoretical models of the developed damper design are presented in this chapter. The first is an analytical model, based on fundamental beam bending equations. A finite element model was also developed by Professor Nam-Ho Kim at the University of Florida. Both these models assume the tool to be a cantilevered beam, and by simulating the actual forces that act on the tool during machining, the models predict the friction work produced due to relative displacement between the tool and the damper fingers.

The damper was primarily designed to fit into the tool through a blind hole made on the shank. When the tool rotates, the centrifugal forces generated at high speeds tend to push the fingers of the damper outwards against the inner surface of the tool shank. During this event, when the tool experiences bending vibrations, the fingers slide over the inner surface of the tool body. The relative sliding is proportional to the distance from the neutral axis of the tool to the neutral axis of the individual fingers. The frictional forces, which arise during this sliding of the fingers over the inner surface of the tool body, dissipate energy and produce damping. Figure 3-1 shows two different centrifugal dampers.

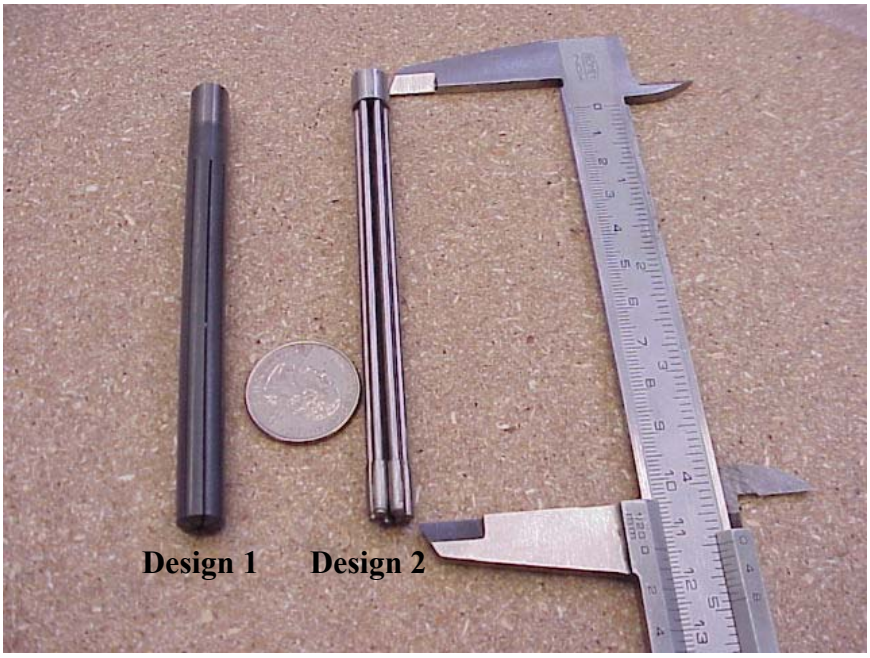

Figure 3-1. Centrifugal dampers.

Two designs of the damper were developed in this research. The first one was developed by Sterling [12]. The second is a modified design, which was developed to attempt to improve the damper performance. Since both the designs were based on same fundamental concept, the basic equations for calculating the friction work remain the same except that the second model has a much-simplified geometry and assumes that the contact between the tool's inner surface and the damper is only at the end. The equations for calculating the frictional work will be derived for the original model followed by the modified equations that were used to calculate the frictional work of the new design.

Analytical Model

In order to help the reader understand the analytical model, Figure 3.2 shows only one finger of the damper. The damper can be designed with any number of fingers in order to obtain maximum energy dissipation.

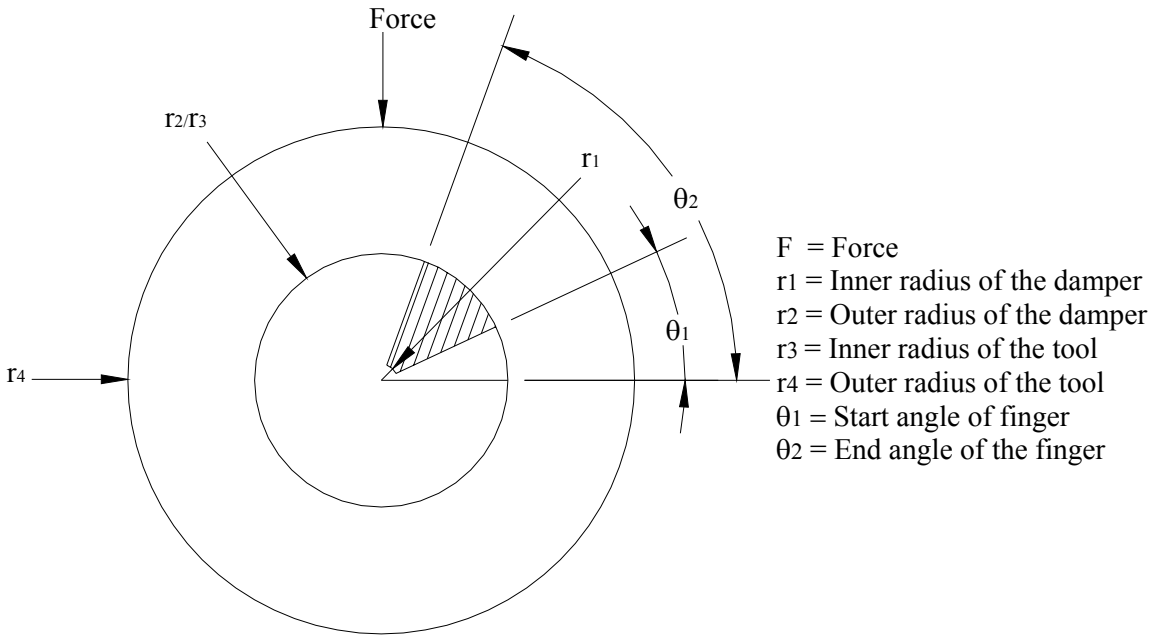

Figure 3-2. Sectional view of the tool and the damper assembly.

The damping caused by the structure in the model is due to the principle of axial shear in beams. It is well known from the elementary engineering subject called Mechanics of Material, that beams undergo internal shear deformation along their axes during bending. Members of a composite beam that are not securely fixed together will slide over each other in proportion to their distance from the neutral axis of the composite beam. It is this same sliding which would occur in the model beam while bending as long as the neutral axis of the internal members, or fingers, does not coincide with the neutral axis of the composite beam [12].

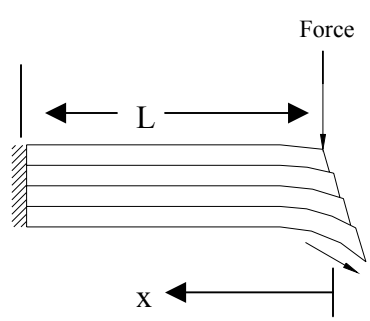

Figure 3-3. Bending in a layered cantilever beam.

When a point load similar to the one shown in Figure 3-2 and Figure 3-3 acts at the end, the deflection at any point on a single cantilevered beam is given by the equation

$$\Delta = \frac{F}{6EI}(-x^3 + 3xL^2 - 2L^3) \tag{1}$$

where

F-force acting at the tip of the beam

E-Young's modulus of elasticity

I-moment of inertia of the beam

L-length of the beam

x-position along the length of the beam

When a composite beam as shown in Figure 3-3 is subjected to a similar force, all the members of the beam will experience the same deflection. Assuming F_t to be the portion of the applied force required deflecting the tool shank; and F_f to be the portion of the applied force required to deflect the damper fingers. E_t and E_f, the Young's moduli of the tool and the damper respectively. I_t, the moment of inertia of the tool and I_f the moment of inertia of the damper relative to the tool centerline. The deflection on the beam is given by

$$\Delta = \frac{F_t}{6E_tI_t}(-x^3 + 3xL^2 - 2L^3) = \frac{F_f}{6E_fI_f}(-x^3 + 3xL^2 - 2L^3) \tag{2}$$

The above equation shows the individual forces acting on the tool and the damper. The total force acting on the composite beam is the sum of the forces required to deflect the individual elements.

$$F = F_t + \sum F_f$$

For the initial analysis, assuming a damper with two members inside the tool, and using equation (2)

$$\frac{F_t}{E_t I_t} = \frac{F_{f1}}{E_{f1} I_{f1}} = \frac{F_{f2}}{E_{f2} I_{f2}} = \Delta$$

Rearranging the equations,

$$F_t = \frac{E_{f1} E_t I_t}{E_{f1} I_{f1}} \tag{3}$$

$$F_{f2} = \frac{E_{f1} E_{f2} I_{f2}}{E_{f1} I_{f1}} \tag{4}$$

Substituting these in the equation for total force,

$$F = F_t + F_{f1} + F_{f2}$$

Substituting equations (3) and (4) into the above equation,

$$F = \frac{E_{f1} E_t I_t}{E_{f1} I_{f1}} + F_{f1} + \frac{E_{f1} E_{f2} I_{f2}}{E_{f1} I_{f1}} \tag{5}$$

Solving for F_{f1}

$$F_{f1} = \frac{F E_{f1} I_{f1}}{E_t I_t + E_{f1} I_{f1} + E_{f2} I_{f2}} \tag{6}$$

For the general case of a damper with *n* fingers, the following equations for the forces can be obtained

$$F_{fi} = \frac{F E_{fi} I_{fi}}{E_t I_t + \sum_{i=1}^{n} E_{fi} I_{fi}} \tag{7}$$

$$F_t = \frac{F E_t I_t}{E_t I_t + \sum_{i=1}^{n} E_{fi} I_{fi}} \tag{8}$$

The equation for the relative displacement between the tool and the damper fingers will be derived now. The normal stress on the surface of a cantilever beam is given by

$$\sigma = \frac{Fxc}{I} \tag{9}$$

where

σ-Stress

F-force on the free end

x-position along the beam from the free end

c-distance from the beam's neutral axis to the surface

I-moment of inertia of the cross-section

The axial strain on the surface is

$$\varepsilon = \frac{\sigma}{E} = \frac{Fxc}{EI} \tag{10}$$

When this equation is applied to the damper fingers, c is the sum of d, the distance from the neutral axis of the finger to the neutral axis of the composite beam, and y, the distance between the neutral axis of the finger and the point of interest on the finger surface. The axial displacement of any point on the beam surface is obtained by integrating the axial strain, in this case is from the free end to the point of interest

$$\delta = \int \varepsilon(x)dx \tag{11}$$

Using equation (10) in (11)

$$\delta_{taxial} = \int_{x}^{L} \frac{F_t x(d+y)}{EI} dx$$

Further expanding

$$= \frac{FE_t I_t}{E_t I_t + \sum_{i=1}^{n} E_{fi} I_{fi}} \frac{(0+y)}{2E_t I_t}(L^2 - x^2)$$

$$= \frac{F(y)(L^2 - x^2)}{2(E_t I_t + \sum_{i=1}^{n} E_{fi} I_{fi})} \tag{12}$$

Similarly, the axial deflection of the fingers is

$$\delta_{f1axial} = \int_x^L \frac{F_i x(d+y)}{EI} dx$$

$$\delta_{f1axial} = \frac{F(d+y)(L^2 - x^2)}{2(E_t I_t + \sum_{i=1}^{n} E_{fi} I_{fi})} \tag{13}$$

The relative sliding is the difference between the horizontal displacement of the tool and the fingers at a given point. The friction work of the damper is obtained from this relative displacement multiplied by the friction forces acting between the tool and damper finger. The relative axial deflections is given by

$$(\delta_{f1axial} - \delta_{taxial}) = \frac{F(d+y)(L^2 - x^2)}{2(E_t I_t + \sum_{i=1}^{n} E_{fi} I_{fi})} - \frac{F(y)(L^2 - x^2)}{2(E_t I_t + \sum_{i=1}^{n} E_{fi} I_{fi})}$$

The work done through this displacement is by friction. It is obtained by multiplying the frictional force (friction coefficient, times the normal force, which is the force/unit length at a point times the differential length) with the relative displacement [12] and integrating over the beam length. Thus, assuming the pressure to be uniform over the entire area of the finger, the friction work is

$$W = \mu.P(\delta_{f1axial} - \delta_{taxial})\, dx = \int_0^L \mu.P \frac{Fd\left(L^2 - x^2\right)}{2(E_t I_t + \sum_{i=1}^{n} E_{fi} I_{fi})} dx \tag{14}$$

Integrating the above equation,

$$W = \frac{1}{3}\mu P\left(\frac{FdL^3}{(E_t I_t + \sum_{i=1}^{n} E_{fi} I_{fi})}\right)$$

This is the work done by friction for a displacement at the end of the beam by a specified force, F was assumed to be 100N for a general case.

Notice, the term *P* here is the force acting over unit length. This happens to be the centrifugal force caused by the rotation of the spindle. It is obtained by dividing centrifugal force by the total length of the damper. The values generally depend on the spindle speed. For this model the spindle speed was assumed to be around 26000 rpm which produced a *P* value of approximately 8000 N per unit length.

For the damper developed by Sterling [12], the friction work is calculated by integrating over the full length of the beam; since the damper contacts the inner surface of the tool over its entire length. In the second design, the fingers are designed to contact the inner surface of the tool only at its free end, where the relative displacement is maximum. It is also assumed that the total centrifugal force on the finger is split evenly between the fixed end of the finger and the free end. Thus the friction work is obtained by considering the relative displacement only at the tip or the free end. Therefore, for this design the integration over the entire length of the beam need not be done. The friction work becomes

$$\mathrm{W} = \frac{1}{2}\mu P\left(\frac{FdL^2}{(E_t I_t + \sum_{i=1}^{n} E_{fi} I_{fi})}\right)$$

The expression to find the moment of inertia I_f of the fingers and I_t of the tool, the distance *d* between the neutral axis of the finger and the neutral axis of the beam, the

volume and the contact force *P* for both the designs are derived and presented in Appendix A.

Calculation of the friction work done by the damper was done using Matlab. Codes were written to vary the physical dimensions of the damper to arrive at optimal design parameters. The code assumed the model to be static, meaning that a constant force was applied at the end of the tool and the work done during deflection by one finger was calculated, although, centrifugal forces were included in order to give more realistic boundary conditions.

The tool chosen for research was a 3/4" dia, 5 inches long, high-speed steel 3-fluted end mill. High-speed steel was chosen because it was easier to make blind hole on the shank and is very cost effective. A blind hole of 4 inches in depth was made on the tool shank; this was made to ensure that there was enough material on the end of the shank to grind the flutes. This also protects the damper from the chips created during machining, which could affect the damper performance by getting in between the fingers. Based on these constraints it was decided that the diameter of the blind hole should be 3/8”. The damper designed to fit in to this hole was made of carbide due to its higher density. The damper was made from a single carbide blank of 0.375”dia and 4 inches in length. The blank was machined to give it a light press fit when inserted into the blind hole of the tool. The fingers were made by slitting the blank with wire EDM, leaving 1 inch at the end unslit for the press fit into the tool.

Figure 3-4 shows the frictional work done by the first damper design with increasing number of fingers. It was found that the work done did not change significantly beyond 8 fingers.

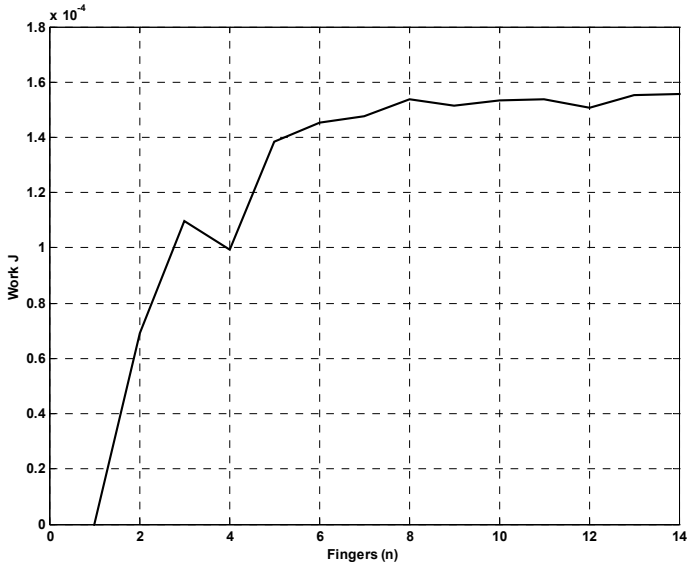

Figure 3-4. Frictional work done by damper made of carbide.

From the derivations presented earlier, it can be seen that increase in *d*, the distance between the neutral axes of the finger and the shank, will increase the frictional work done because of larger relative sliding between the members. This can be accomplished by fabricating the damper with a inner hole, at the cost of lower centrifugal pressure on the interface. To investigate the effect of inner holes in the damper, the value of r_1 was increased from zero to see if there is any significant change in the magnitude of work produced. It was found that there was no significant change in work for small central holes. As the hole diameter became larger, the friction work started to decrease due to loss in finger volume. Therefore it was decided to fabricate the dampers with no inner hole. The friction work obtained from this model also depends on the start angle of the fingers. The plots below show that the magnitude of the work done did not significantly change beyond 8 fingers regardless of the start angle. Therefore it was decided to use an eight-fingered damper for the experimental tests.

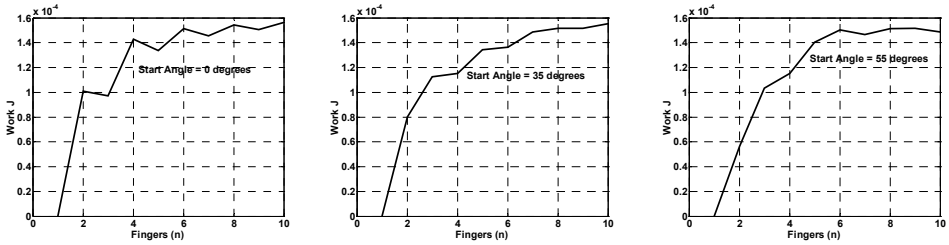

Figure 3-5 Frictional work obtained with 0° (left), 35° (center), and 55° (right) start angles.

One result of the initial analysis was the realization that the maximum sliding distance between the tool and damper finger occurred at the free end. At all other points, the sliding distance was less. Therefore, a second design was developed in which the finger shape was modified so that it contacted the tool surface only at the fixed and free ends. The new damper was also designed to have a larger distance between the two neutral axes and to make it cost effective was made from stainless steel. The damper is shown in Figure 3-1 on the right hand side. The damper consists of three components namely the base, the rods or fingers that fit into the base, and the sleeves that slides over each finger. The components were designed to have a light press fit when assembled.

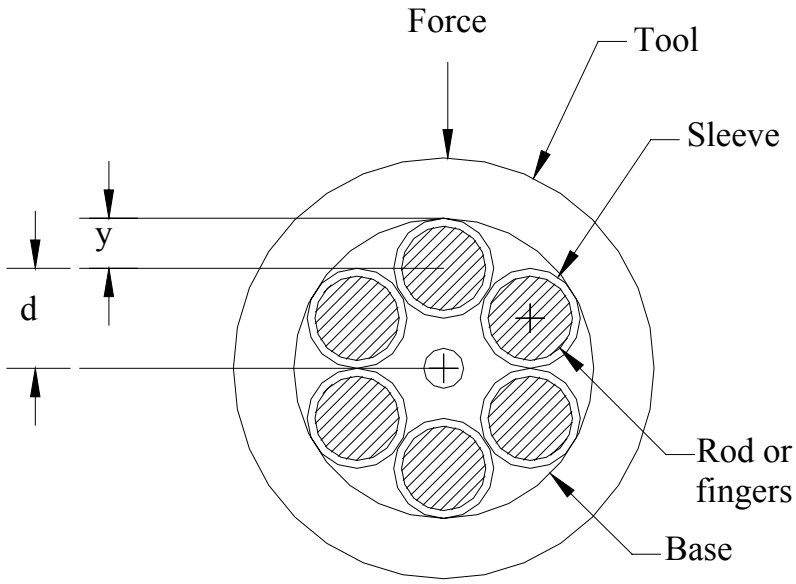

Figure 3-6. A sectional view of the tool and the new damper assembly.

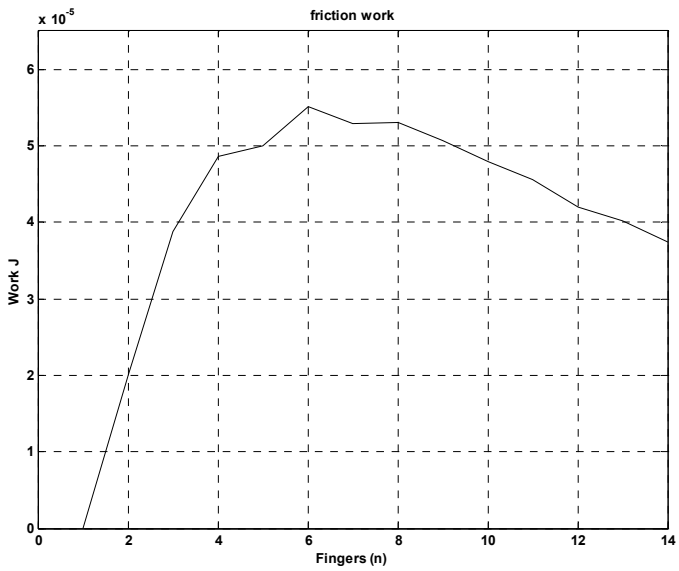

Figure 3-7. Variation in frictional work produced by the damper made of stainless steel.

The frictional work done by the damper is shown in Figure 3-7. Similar to the first design, codes were written in Matlab and the physical dimensions of the damper were varied to obtain maximum work. It was found that for the given dimensional constraints and variations in start angles, a six-fingered damper produced the maximum work. This was chosen as the optimal design for the damper.

It can be noticed from Figure 3-4 and Figure 3-7 that the predicted frictional work done by the second design is much less than the first. This result was confirmed by subsequent cutting tests. It was found that although the second design did marginally better than the solid tool with no damper, the material removal rate when compared to the first design was much less. Possible reasons for this poor performance could be, the difference in the density of the damper materials used and loss in volume due to change in geometry, which led to significantly smaller centrifugal forces on the fingers. Even though, the sliding distance at the contact zone was larger, it wasn't enough to compensate for the lower contact forces. Based on these initial results, the initial damper

design made of carbide was found to perform better, and was chosen to complete the rest of the research work.

Finite Element Model

Finite element analysis is widely used to analyze complex systems for stress and displacement. Professor Nam-Ho Kim at the University of Florida developed the FEA model of the centrifugal damper and used it to calculate the frictional work produced by the damper. ANSYS was used to perform the analysis. The damper model was created as an extruded cylinder slit along its length and was assembled coaxially inside a hollow shaft.

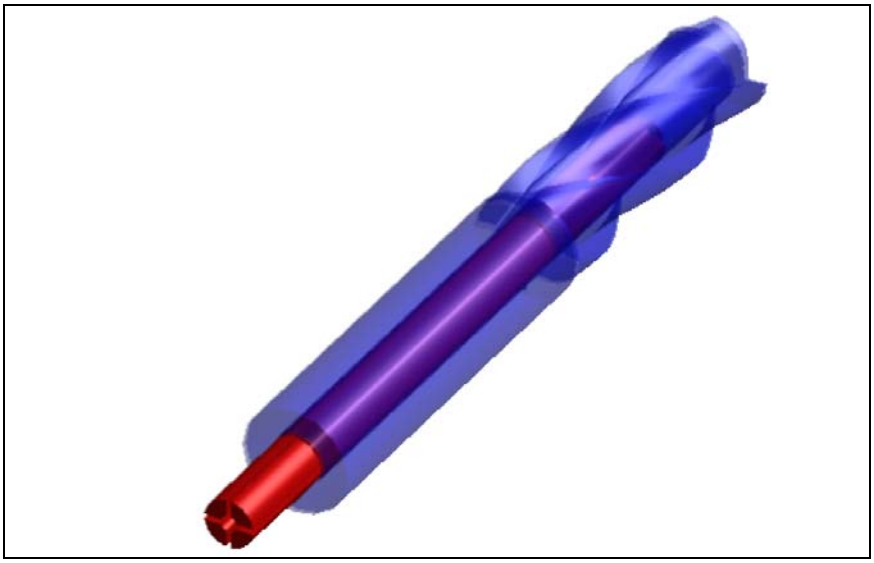

Figure 3-8. Solid model of the tool and damper created by Professor Kim using ANSYS.

8-node contact pairs were created between the tool and the damper interface. A 20-node cubic element was created and used as solid mesh elements in the model. Similar to the analytical model, the tool and damper assembly was assumed to be a composite cantilevered beam. To create the effect of the centrifugal force, a rotational velocity of

2723 rad/s was added with a vertical force of 100N at the free end of the tool. The friction coefficient used was 0.15.

In order to compare the results of the finite element model with that of the analytical model the first geometrical design was chosen for analysis with similar material properties. The Young's Modulus was 206780 MPa, the mass density was $7.82 \cdot 10^3$ kg/m^3, and the Poisson's ratio was 0.29.

The friction work was computed by taking the dot product of the nodal forces and the relative nodal displacements at the interface. The physical dimensions of the model were optimized to obtain the maximum work.

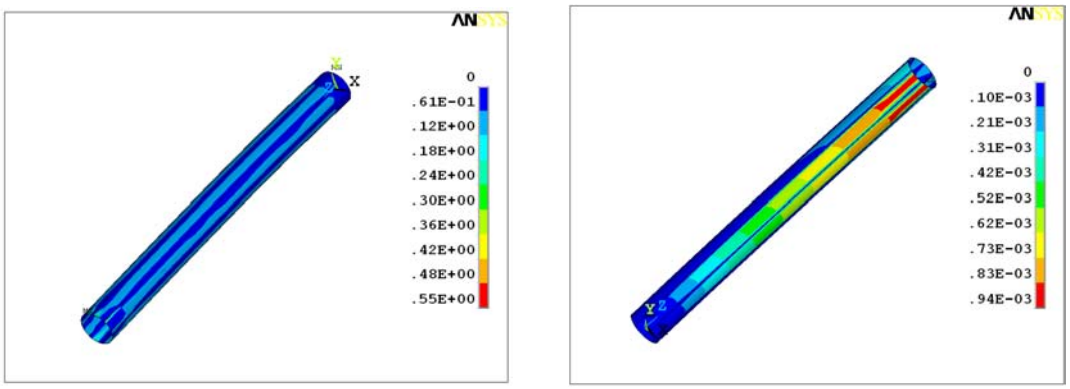

Figure 3-9. Friction stress (left) and relative displacement (right) obtained from ANSYS.

The friction stress and the relative displacement from the finite element model of the damper are shown in Figure 3-9. The final results of the calculations are shown in Figure 3-10.

Comparing the work magnitudes of both the models shows that the frictional work calculated by the analytical method is greater than the finite element model. Although there are only a small differences in values, the results clearly shows the assumption

made by the analytical method that the relative displacement occurs over the entire length of the beam has overestimated the work output.

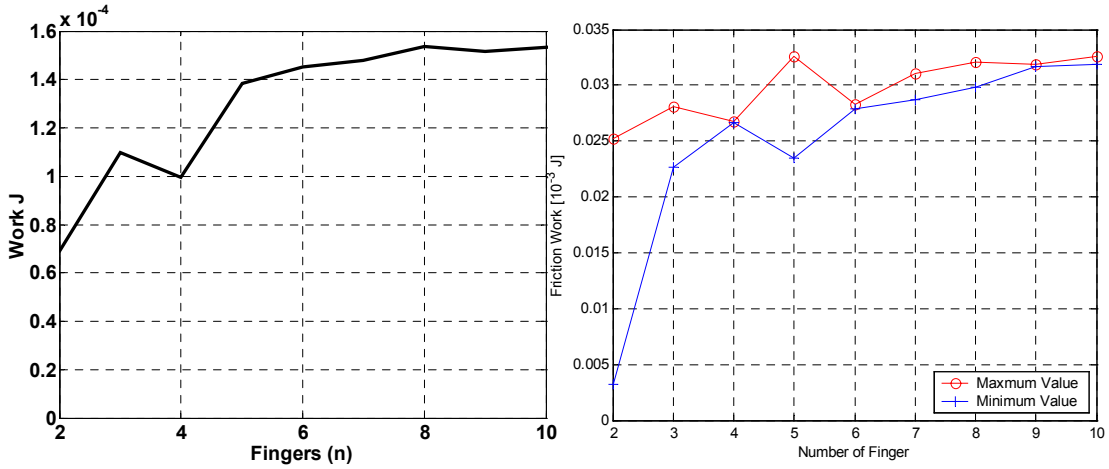

Figure 3-10. Comparison of frictional work done by analytical method (left) and finite element approach (right).

While the results obtained from the theoretical model explain the behavior of the damper inside the tool, cutting tests must be performed on the tool-damper assembly to see the effect of the damper on tool stability. The next chapter explains the instrumentation and test setup used for measuring the frequency response functions of the spindle and tool along with the procedure to create stability lobes from these measurements.

CHAPTER 4
TOOL CHARACTERISTICS AND STBILITY LOBES

Frictional work predicted from the theoretical model is just an approximation of work magnitude that could be obtained from the damper design. This is because theoretical models sometimes tend to overlook the actual testing conditions and may result in overestimating the values. To verify the analytical results cutting tests were performed. A detailed description of the experimental setup, instrumentation and tests conducted to measure the FRF of the tools used will be presented in this chapter.

Modal Testing

Modal analysis is defined as the study of the dynamic characteristic of a mechanical structure. When an external force excites a mechanical structure, the energy that is stored within the structure, during excitation, is given out at its natural frequencies. This is exhibited through different mode shapes of the structure. In this research, modal testing is used as a preliminary experiment to understand the tool behavior when static and during rotation. The experimental setup for modal analysis is shown in Figure 4-1.

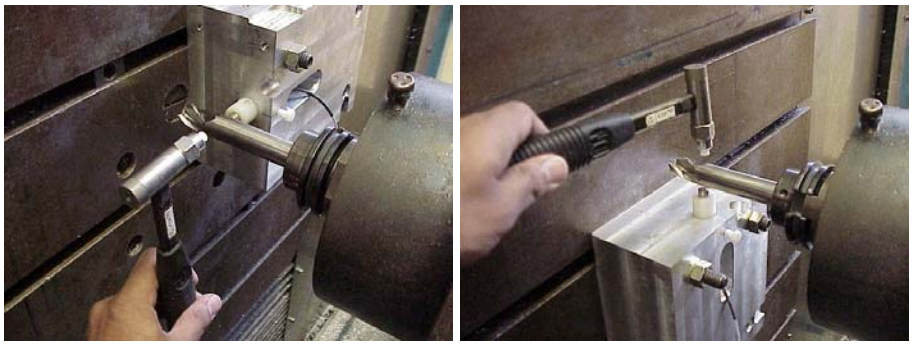

Figure 4-1. A setup showing the modal testing being performed on a tool in x (left) and y (right) directions using an impact hammer and cap probe.

A modal testing setup primarily consists of an exciting device, a transducer and an analyzer to see the response of the structure. In this case, the structure is a tool. The measurements are typically done by mounting the tool on to the holder spindle assembly, and then exciting the tool with a modal hammer and recording the response from the transducer.

The modal hammer is a commonly used device to excite a structure. It is a simple instrument that measures the amount of force applied to the tool through a load cell inside [12]. Since force is an impulse, the amplitude of the energy level applied to the tool is a function of mass and velocity of the hammer.

The transducers used to measure the response of a structure are categorized into two types, the contact and the non-contact type. The accelerometer or a piezoelectric transducer is an example of a contact type transducer. It is an electromechanical sensor that generates electrical output when subjected to vibrations. The piezoelectric crystal present inside accomplishes this by giving out electrical charges in one direction when strained on the other (normally perpendicular). When the accelerometer vibrates, force is applied through an internal mass over the crystal, which is proportional to the acceleration. The analyzer then records this response as voltage measured from the accelerometer. This type of transducer is generally preferred to other types because it has a wide frequency and dynamic range, good linearity, and is relatively durable.

Examples of non-contact transducers are the capacitance probes and a laser vibrometers. A capacitance probe measures displacement directly from the structure whereas a vibrometer measures the velocity. In the current research a capacitance probe was used because rotating FRFs had to be measured.

The capacitance probe works on the principle, that, when two conducting materials are separated by a dielectric medium (generally air) in between them, the change in capacitance is measured as,

$$capacitance = \frac{area \cdot dieletric}{distance}$$

Here, area refers to the size of the target. When the area and the dielectric medium are held constant the change in capacitance is only a result of change in distance between the probe and the target material. With proper instrumentation, a voltage corresponding to the distance can be obtained. For this research a capacitance probe setup with a sensitivity of $2.5 \cdot 10^{-5}$m/volt was used.

A dual-channel dynamic analyzer was used to record the data. The analyzer has the capacity to trigger its own source such as white noise, swept sine, chirp signals, and so on. It can also perform curve-fitting operations. Frequencies of up to 102.6 KHz can be analyzed with a single channel amplitude accuracy of up to 0.2dB.

Test Setup

The experimental setup to measure the dynamic characteristics of the tool are shown in Figure 4-1. One of the objectives in developing the damper is to implement it on a commercially available cutting tool, but in the current research, to initially observe the damper performance, tools of specific geometry were fabricated and used for testing. The tools designed for the experiments were 127mm long, 19.5mm diameter, and 3 fluted high-speed steel end mills with Young's Modulus of 20GPa, and a density of 7820 kg/m^3. To observe the effect of the damper on the tool, one tool was made out of solid blank and the other tool on a blank with a blind hole to fit the damper. The blind hole made on the

shank was 9.5mm in diameter and 102mm deep. The flute length on the tool was 25.4mm.

Selecting The Right Tool Overhang

The length of the tool overhang from the holder was considered to be a very important factor when analyzing the tool characteristics. Research done by Schmitz and Donaldson [5] showed that changing the lengths of the tool overhang from the holder spindle assembly affects the dynamic characteristics of the entire system. For this reason, and in order to obtain a dominant mode of the tool in the FRFs, different tool overhangs were tried to see if there was any region where the tool mode could be observed without interacting with other spindle modes.

High-Speed Spindle

Setco, Inc. developed the spindle currently being used on High-Speed Machine (HSM-1). The spindle can achieve a maximum speed of around 36000 rpm. The spindle has a power requirement of 1KW per 1,000 rpm, which produces a torque of 10 Nm. A sectional drawing of the spindle is shown in Figure 4-2.

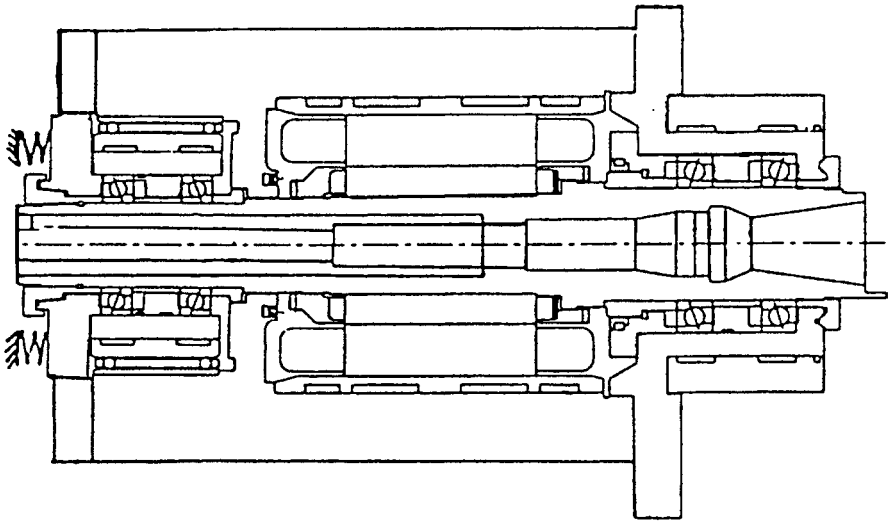

Figure 4-2. Cross-sectional view of the HSM-1 spindle with constant preload.

The high-speed spindle has two pairs of hybrid angular contact bearings composed of silicon nitride balls on steel inner and outer races. Springs acting on the floating mount supporting the rear pair of bearings provide a constant axial preload to the spindle. A rotor of an induction-type motor is mounted on the spindle shaft and is driven by a frequency converter power supply. Currently, the working range of the spindle is roughly 20,000 rpm to 30,000 rpm. This was the spindle used for the current research.

The tool holder used in the spindle is a CAT40 thermal shrink-fit type holder. These types of holders need to be balanced to remain stable at higher spindle speeds. Initially, measurements were made on the spindle alone, to find out the natural frequencies and mode shapes. For this, the holder was mounted without the tool onto the spindle and the non-rotating FRFs were measured using a modal hammer and accelerometer.

Overhang Length

The frequency response function of the spindle in x-direction is shown in Figure 4-3. From the plots it can be seen that the natural frequencies of the spindle are around 780 Hz, 885 Hz, and the 1410 Hz. These frequencies clearly indicate that any wrong judgments in the tool overhang length made, will result in interacting modes and would lead to difficulties in understanding damping effects on those modes at later stages.

Taking this into consideration, selection of tool lengths were made to avoid any interaction with the existing modes. After performing careful measurements, it was found that an overhang of 4” would be the best length to observe the tool characteristics. The FRF of the holder spindle assembly is shown in Figure 4-4.

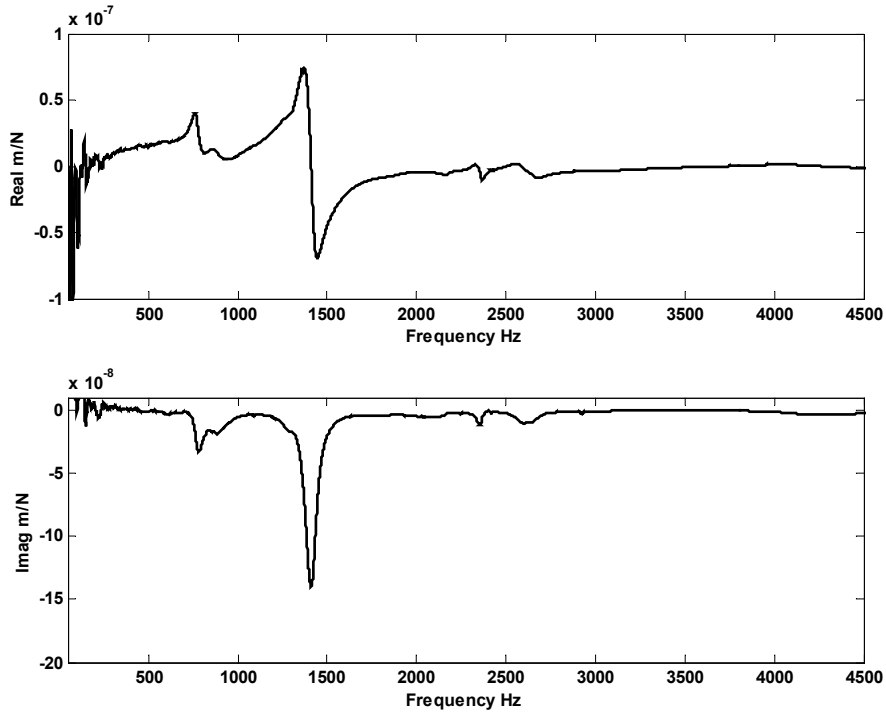

Figure 4-3. FRF of the holder-spindle in x-direction.

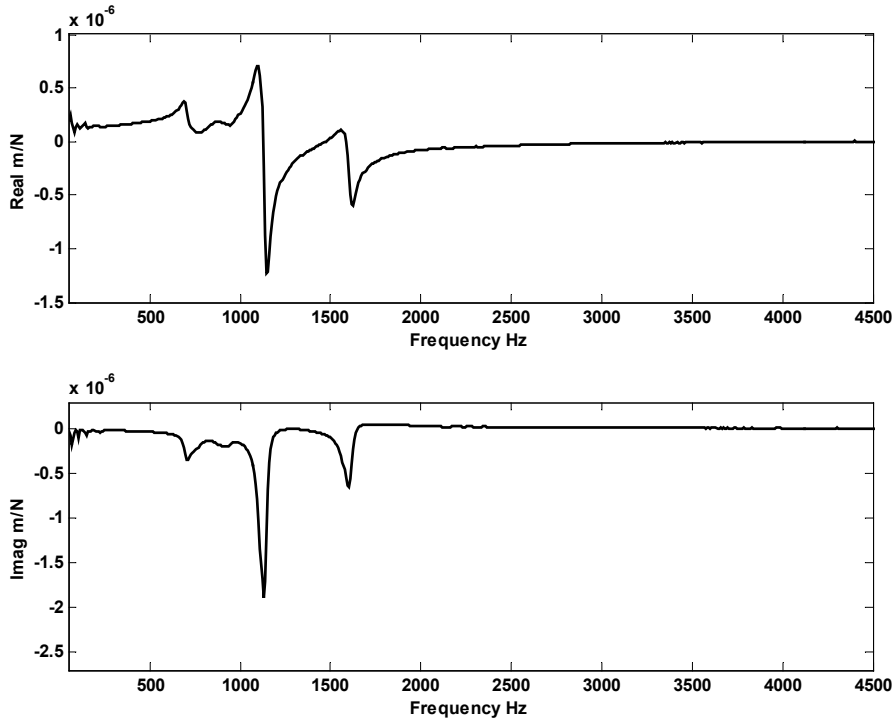

Figure 4-4. Static measurement of a ¾” 3-fluted H.S.S end mill in x-direction.

It can be seen from Figure 4-5 that at around 1100 Hz, a new mode appears in the middle of the existing modes. It was also interesting to note that this new mode shifted the mode that was initially at 1410 Hz to 1600 Hz. Though the chosen length seemed to have had a marginal effect on the existing modes, it was still considered to be the best overhang length to observe the behavior of the tool while testing it with the damper. Similar behavior was noticed in the y-direction. Figure 4-5 and 4-6 shows the FRFs measured in the y-direction.

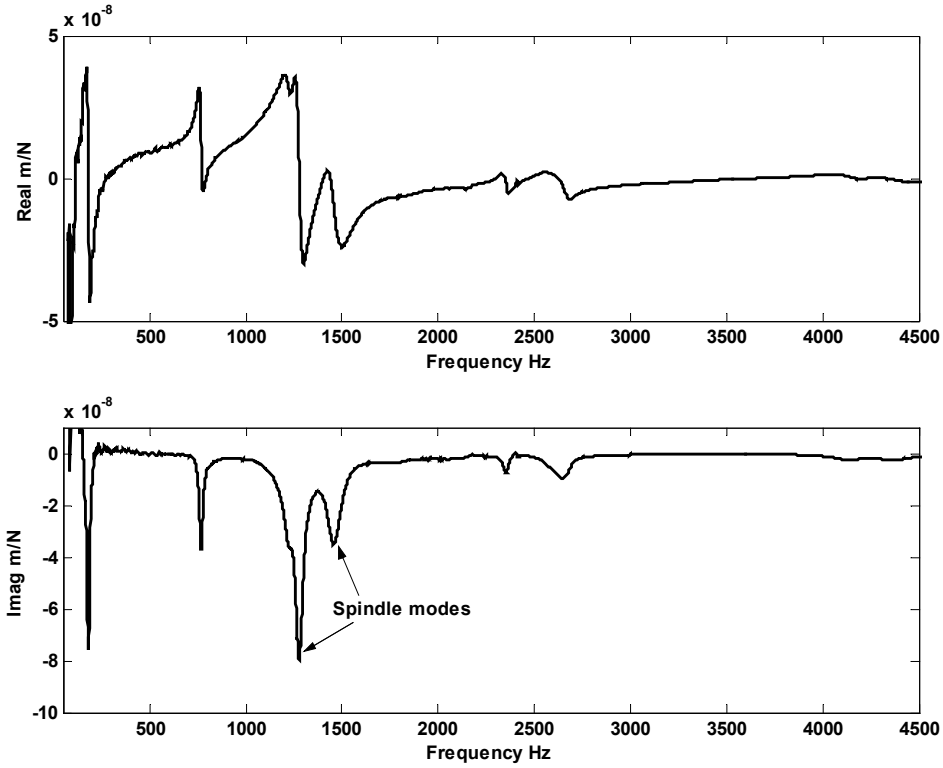

Figure 4-5. FRF of the holder spindle in y-direction.

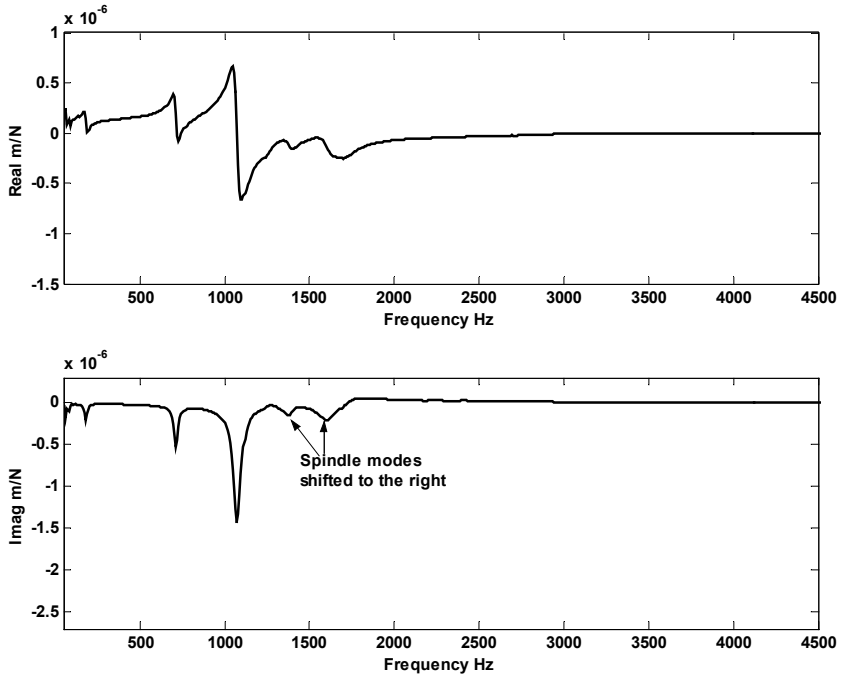

Figure 4-6. Static measurement of a ¾" 3-fluted H.S.S end mill in y-direction.

In all these measurements, care was taken to achieve a constant torque when mounting the holder on the spindle to avoid any uncertainty in the measurements.

Three types of tools were used for measurements. A solid tool, a hollow tool with a blind hole of 4" deep and later the same hollow tool was inserted with damper and tested again.

Effect of Spindle Speeds on FRFs of The Tool

Stability lobes for a tool are typically generated from modal parameters obtained from static measurements; this was a common practice because, generally, the spindle dynamics were not expected to change with speed or temperature. However, during this research, it was observed that there was a change in the dynamic stiffness of the tool while measuring the frequency response functions (FRFs) at different speeds. It was quite interesting to observe that the magnitude of response of the tool mode kept decreasing at

higher spindle speeds. This observation motivated a study of the spindle and tool characteristics at different speeds. This section outlines the procedure followed to obtain the frequency response functions of the tool at various spindle speeds. Later, these obtained FRFs at different speeds will be used to generate stability lobes and will be superimposed on the lobes generated from static measurements to show the effect of the spindle speeds on these measurements.

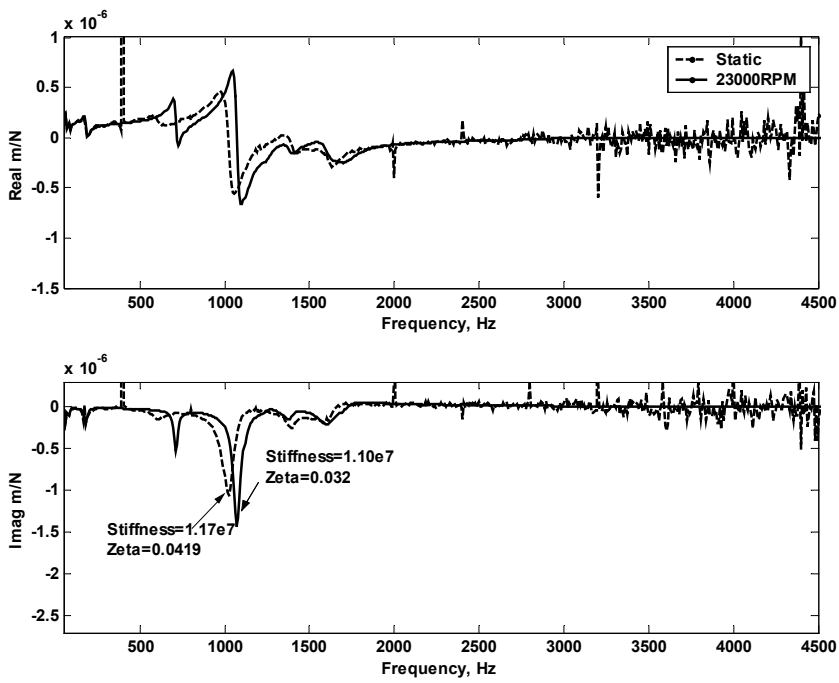

Figure 4-7. Response of solid tool at two different spindle speeds in Y-direction.

Stability Lobes

Stability lobes are plots that map the relationship between the axial depth of cut and the spindle speeds. These lobes are developed from the modal parameters obtained from the FRFs of the tool. The formula for calculating the axial depth of cut b incase of milling given by Tlusty [2] is,

$$b_{\lim} = \frac{-1}{2mK_s \operatorname{Re}(G)} \qquad 4.1$$

where

b_{lim}	-	Axial depth of cut
K_s	-	Specific cutting energy
Re (G)	-	Real part of the obtained FRF
m	-	Average no. of teeth in the cut

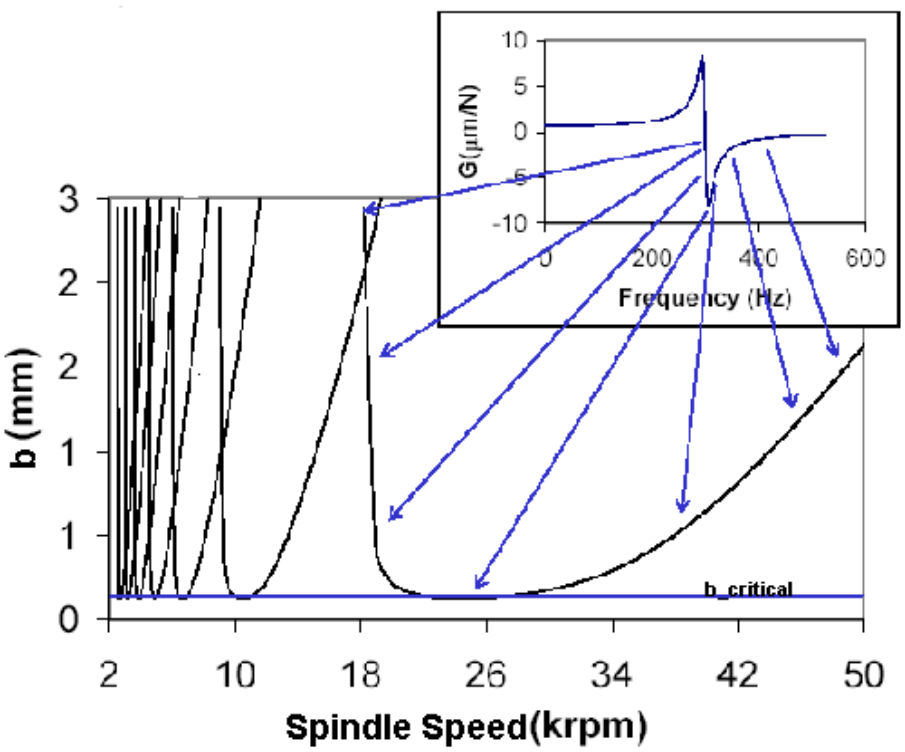

Figure 4-8. Mapping b_{lim} from the FRF obtained.

The above figure clearly shows the points on the stability lobes mapped down from the real part of the FRF. For chip widths $b<b_{lim}$ cutting is always stable: there is no self-excited vibration. For $b>b_{lim}$ the tool starts to chatter [2].

To understand more clearly the way these lobes are plotted, a quick review of the steps involved are given below

The general procedure followed in calculating the spindle speeds and the depths of cut are

1. Pick a chatter frequency from the negative real part of the FRF curve.
2. Calculate the minimum b_{lim} or critical depth from equation 4.1, which belongs to that frequency.
3. For every chatter frequency found from the negative values of the real part, the spindle speeds are found. This is given by the formula.

$$N + \frac{\varepsilon}{2\pi} = \frac{f_c}{m \cdot n}$$

where

N - Integer number of waves

ε - Phase shift between the waves

f_c - Chatter frequency

m - Number of teeth in cutter

n - Spindle speed

4. This procedure is repeated by scanning the chatter frequencies around the natural frequency of the tool [13].

Although the basic steps involved in generating the stability lobes remain same, researchers like Tlusty [2], Tobias, and Altintas [13] generated the stability limits with different theories on the cutting process of the tool. For this research professor Altintas's model was used.

In the method developed by Altintas [13], the force on a tooth of a milling cutter was considered to be varying with its position on the work piece. For a known chatter frequency, cutting coefficients, and radial immersion, his model of the milling process results in a 2-D coupled dynamic eigen-value problem to obtain the axial depth of cut [13]. The model also suggests that by taking the average of individual directional

components and formulating the chatter as an eigen-value model, a more accurate result can be obtained. This is unlike the other models, which approximates the problem as one-dimensional by using average cutting force. Using this method, computer codes were written by Professor Tony Schmitz to generate stability lobes and were used for the research.

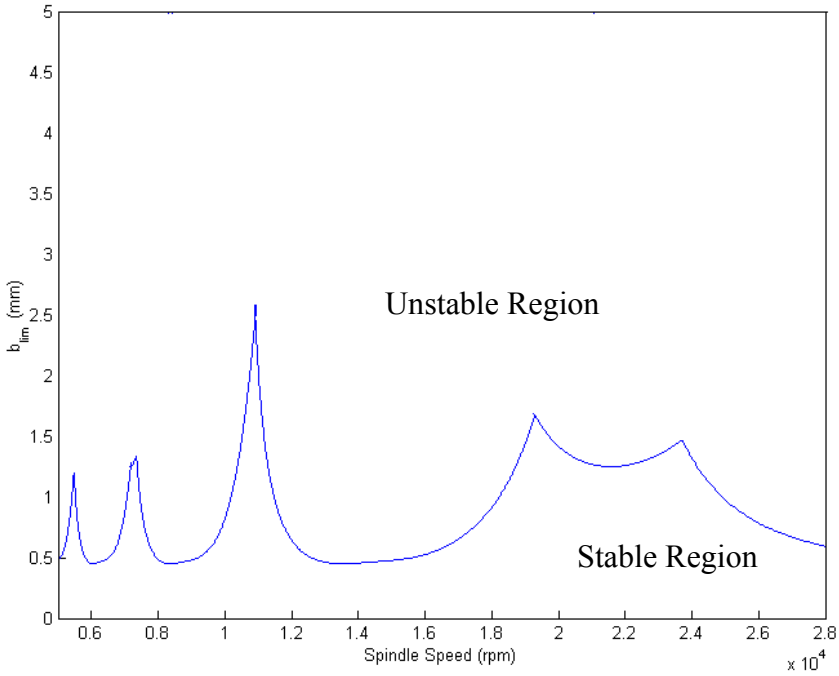

Figure 4-9. Stability lobe diagram of a test tool (FRF measurements taken when spindle at rest).

Measurements

Initially, a solid tool was tested. The procedure involved measuring the FRFs from 10,000 rpm to the working range of the spindle, which was around 28000 rpm. The FRFs were measured at 1000 rpm increments. As mentioned earlier, a cap probe was used to measure the FRFs. It is important to mention here that all the measurements taken were below the flutes of the tool. This is approximately 1.1” from the end of the tool on the shank. The reason was that the cap probe cannot read in the gap between flutes. The

output from the modal hammer and the cap probe was fed into a signal conditioner and then was recorded by the Stanford analyzer.

From the brief description given above, a generalized the measurement procedure can be made,

1. Mount the tool onto the spindle using a known amount of torque applied to the drawbar.
2. Mount the cap probe on a stiff fixture.
3. Position the probe at the same axial position for all tools.
4. Adjust the cap probe distance normal to the tool surface to fall within the working range of the probe.
5. Rotate the tool by hand to see if there is sensor remains within its working range. A change in the sensor reading means a possible tool run out or improper mounting of the probe.
6. Properly ground the tool subjected to measurements.
7. Connect the transducers to the signal conditioners or amplifiers and the output from the amplifiers to the analyzer. Make sure there are no loose connections between the terminals to avoid any noise source.

To avoid noise in the signal, average values of the data were used. In this case an average from 15 samples was used. Care was taken to avoid any over loading or a double impact from the hammer. The procedures were followed in both x and y directions.

The measured data obtained from the Stanford analyzer was later converted into ASCII files. Codes were written in Matlab to process these raw data to obtain the desired FRF. A generalized Matlab code for doing this is presented in Appendix B. Figure 4-10 shows one of FRFs measured from the solid tool.

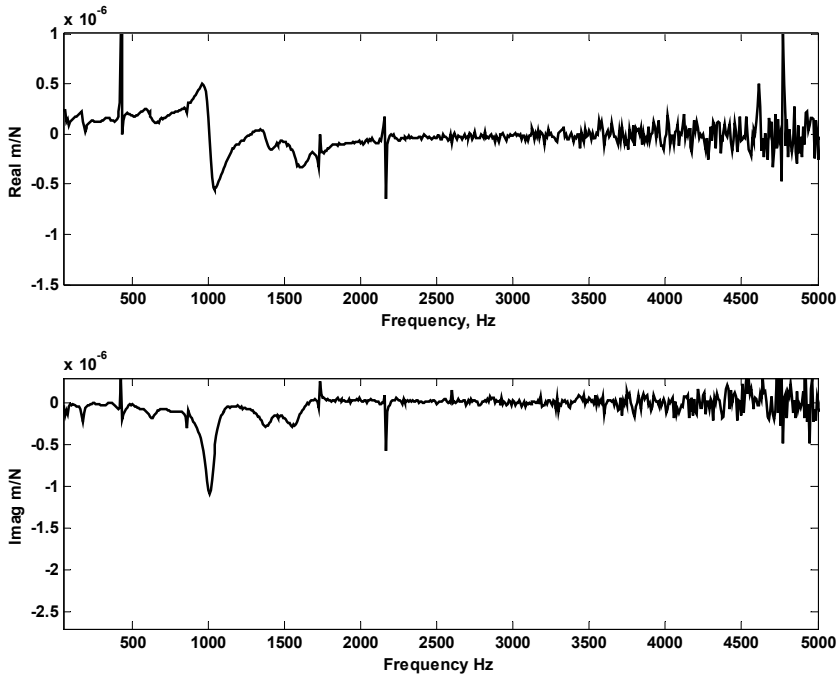

Figure 4-10. Response from a solid tool in y-direction at 26000 rpm.

It can be seen from Figure 4-10 that the response from the tool has frequency contents other than the natural frequencies of the system. One obvious frequency that was observed was the once per revolution signal that appeared due to tool run out. The response shown the figure was obtained at 26000 rpm, which has a runout frequency of around 433 Hz. This is clearly visible on the plot along with its harmonics. Various techniques to filter this noise out were attempted, and it was later found that it was almost impossible to eliminate these frequencies completely.

This problem became a growing concern when the run out frequency and its harmonics fell on top of the modes at certain speeds. This means, the lobes generated at these speeds may not exactly reflect the actual stability limits. As a solution to this problem, equations to generate FRFs with approximate values were initially used to fit the actual measurements. The initial values were obtained from peak picking the frequencies and magnitudes from the actual curves and then calculating the stiffness,

mass and damping ratios from it. Again, codes written in Matlab were used to perform this. The equation used to generate the FRFs was,

$$G = \frac{\omega_{nj}^{\ 2}}{k} \cdot \left(\frac{1}{\left(\omega_{nj}^{\ 2} - \omega^2 + i \cdot 2 \cdot \varsigma \cdot \omega_{nj} \cdot \omega \right)} \right)$$

where,

G = Frequency Response Function of the system

ω_{nj} = Natural frequency, here j depends on the degrees of freedom

k = Modal Stiffness

ζ =Damping Ratio

ω = Variable frequency

The equations to calculate the transfer functions can be expanded depending upon the degrees of freedom in a particular direction, which is x and y. It is also important to mention here that this is the same equation used inside the code for generating the stability lobes.

Having obtained the initial values, a theoretical curve had to be obtained to reflect the actual system. To accomplish this, the initial approximate values were corrected to fit on top of the measured curve. Figure 4-11 shows a generated curve on top of the measured data.

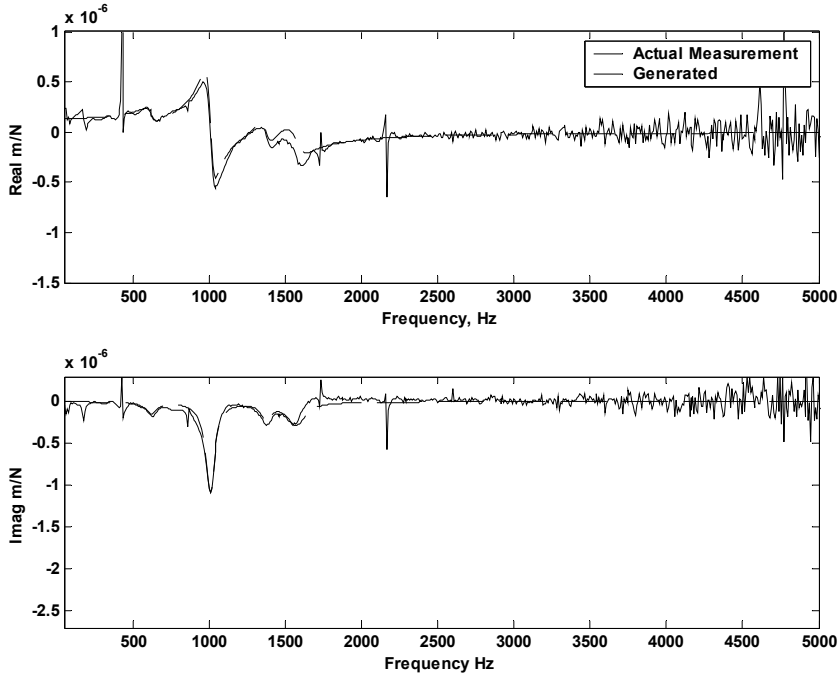

Figure 4-11. A theoretical curve fitted on top of a four-degree freedom system at 26000 rpm.

The procedures discussed so far in this section were carried out for all the measurements taken in both x and y directions for the solid tool.

Projecting the Shank Data

It was mentioned earlier that all the rotating FRFs were measured on the shank of the tool, at some distance away from the end and below the flutes. Since the bending stiffness of the cantilevered tool increases toward its base, it is expected that stability lobes generated from measurements on the shank would be give higher limiting cut depths compared to tool tip measurements.

To project these obtained shank measurements to the tip of the tool. Non-rotating FRF measurements were taken at two places, one at the tip of the tool and the other at the point on the shank where the rotating FRFs were measured.

The measurements were made using an accelerometer and an impulse hammer.

Figure 4-12 shows that magnitude of response of the solid tool in both x and y directions.

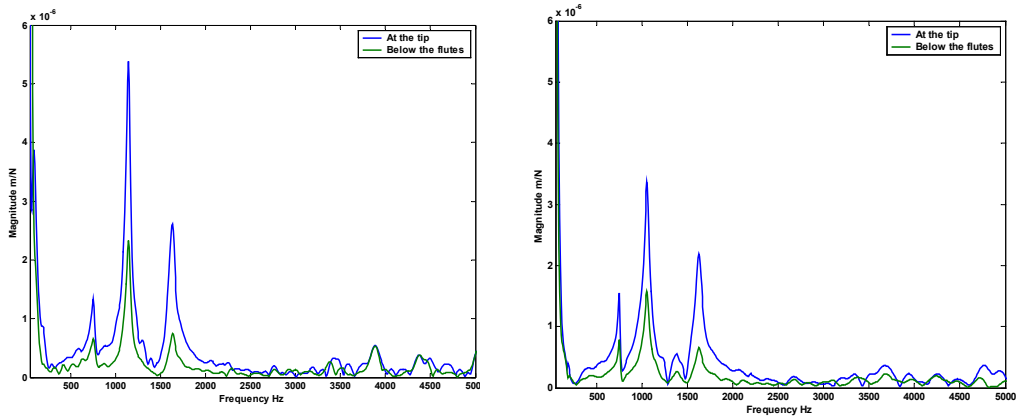

Figure 4-12. Magnitude of response for a solid tool measured in x (left) and y (right) direction.

In order to project the measurements made below the flutes, to the tip of the tool, the ratios between these measurements were found out, by dividing the magnitude of the tip values by the shank values measured below the flutes.

The ratios at each frequency in x and y directions are shown in table 4.1

Table 4-1. Ratio of magnitudes for the tip and shank measurements.

X-direction				
Frequency Hz	752	888	1144	1632
Ratio	2.0341	1.4	2.308	3.5253
Y-direction				
Frequency Hz	752	1056	1384	1624
Ratio	1.976	2.138	2.092	3.36

The ratios obtained from the table were multiplied with the terms corresponding to that frequency on the transfer function equation that belongs to the measurements made below the flutes and was plotted again on top of the tip measurements as shown in Figure 4-14.

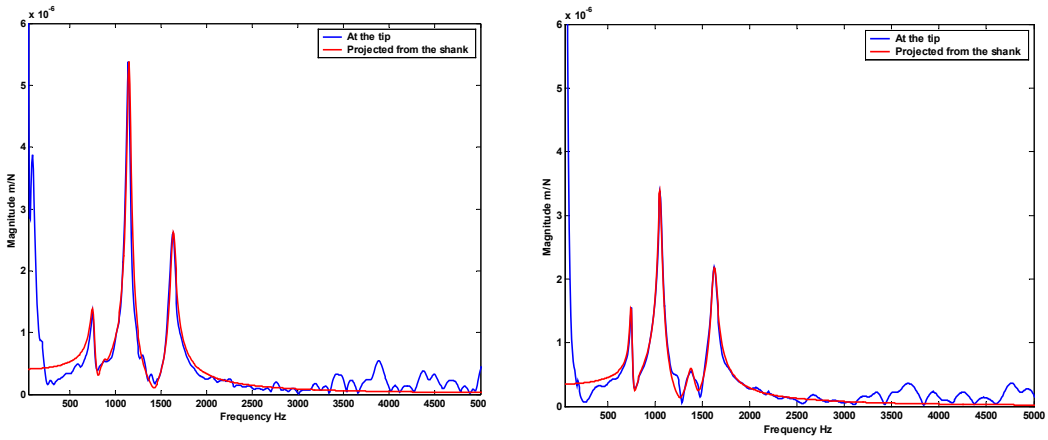

Figure 4-13. Magnitude of the projected values superimposed on the tip measurements.

Plots from Figure 4-13 shows that this approach had a close agreement to what was predicted. To verify this further, stability lobes were generated and plotted to compare the stability limits obtained between these measurements. The code written by Professor Schmitz was used to generate the lobes. The specific cutting energy K_t used for this case was 670 N/mm^2 and K_r was 0.26. A complete immersion or slotting was used as the cutting process in the code.

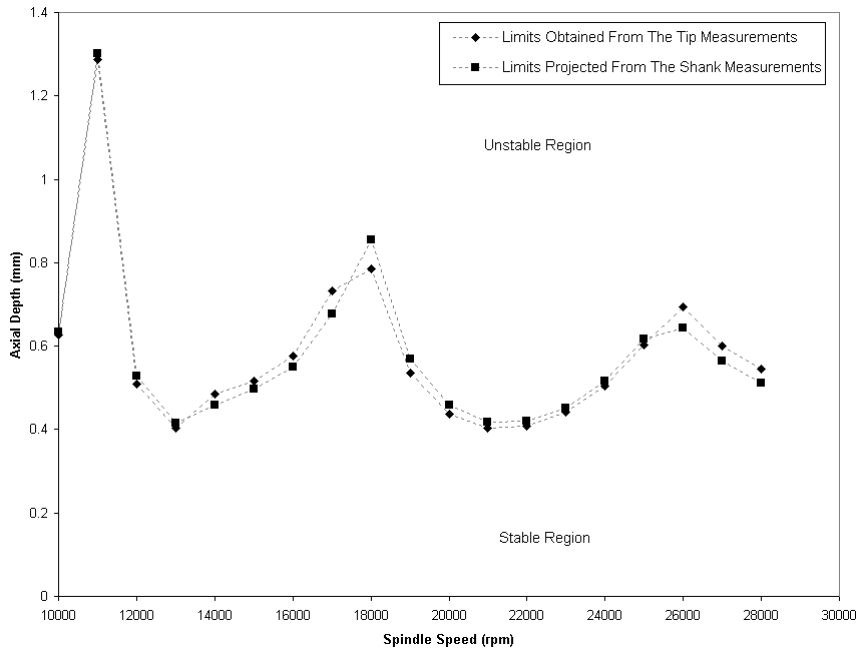

Figure 4-14. Points from stability lobes generated from tip and projected measurements for the solid tool.

Figure 4-14 shows the points taken from the stability lobes generated from the FRFs of the tool tip and the shank. The two sets of points on the plot reveal that the stability limits for both the tip and the projected measurements are almost the same.

Since, these points were obtained from the lobes and are not the actual lobing diagram, it can be noticed that they are discrete in nature. The reason for picking only these points is that, the rotating FRFs measurements in the later part of the experiment were made only at these spindle speeds.

As a next step, the same magnitude ratios were used as a multiplication factor for the rest of the rotating FRFs measurements and stability lobes were generated for speeds ranging from 10000 rpm to 28000 rpm in steps of 1000 rpm. One set of stability lobes for every rpm was generated and the stability limit corresponding to that rpm was chosen as the stable depth of cut at that spindle speed. These points were then plotted as discrete values with straight lines connecting them. Finally, the stability limits obtained from static and rotating FRFs were plotted out to see the effect of spindle speeds on them.

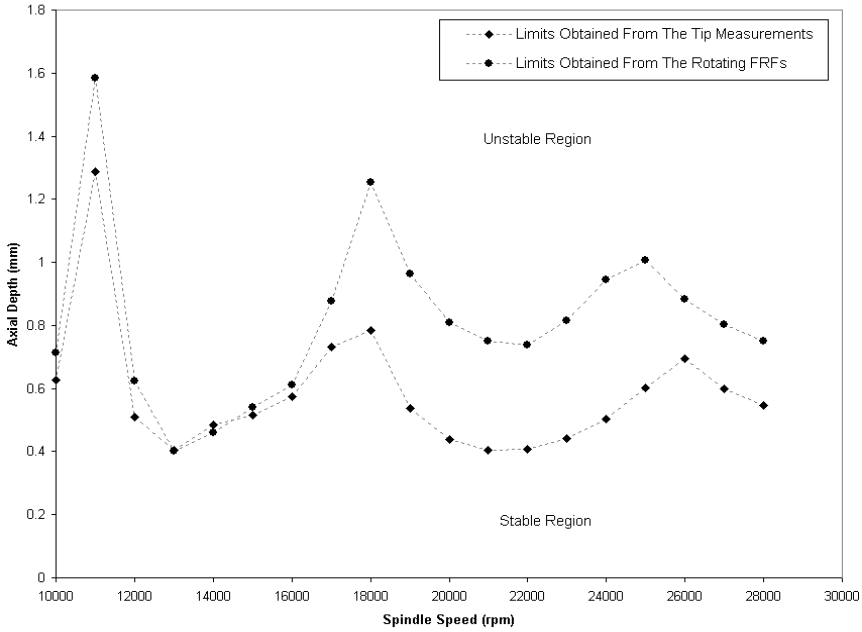

Figure 4-15 Effect of spindle speeds on stability limits of the solid tool.

Figure 4-15 clearly shows that the spindle speeds have shifted the stability limits to a higher value. It can be seen that at lower speeds, there is not much difference between the two plots, but as the speed increases there is a dramatic change in the tool behavior, which is reflected on the stability limit plots seen above.

The reasons for this change in behavior may be due to the change in stiffness of the spindle bearings with increasing speed. This change in stiffness may be due to heat generated at higher speeds and centrifugal forces on the balls in the bearings, which cause the preload and contact angle on the bearings to change, thus changing their stiffness. Also, the centrifugal force due to the spindle velocity along with the change in the temperature would have drawn the holder more tightly into the spindle taper causing a more rigid connection between the holder and the spindle, which would have made the tool stiffer.

The same procedure was followed for the hollow and the damped tool, and the results are shown in Figure 4-16 and Figure 4-17.

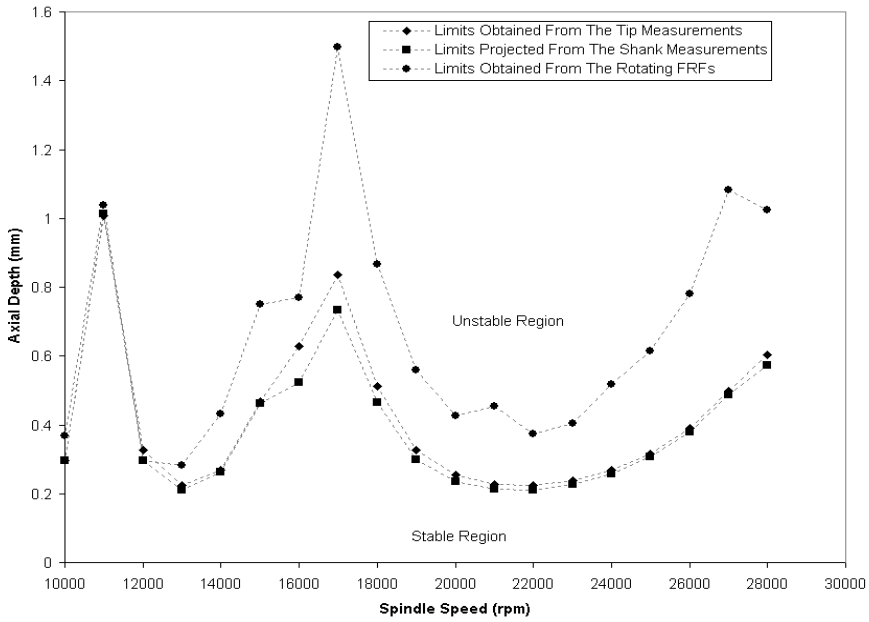

Figure 4-16. Stability lobes for the hollow tool.

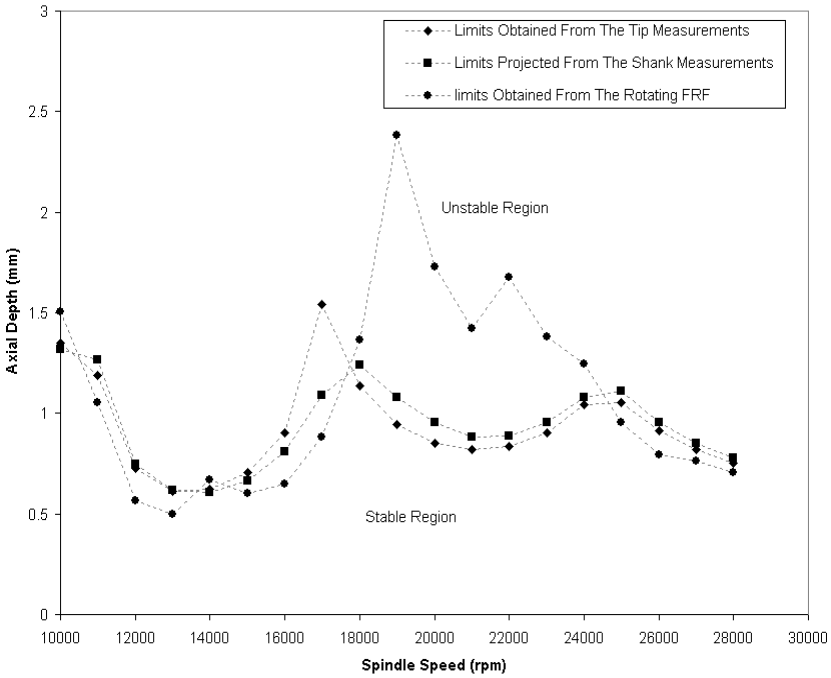

Figure 4-17. Stability lobes for the damped tool.

Thus, a complete set of stability lobes for solid, hollow, and the damped tool were obtained. These lobes were used to plan the cutting tests, which will be presented in the next chapter.

The results of the rotating FRF measurements showed significant changes in the dynamic characteristics of the tool and the spindle at higher speeds, leading to different predictions in stable cutting depths. Cutting tests were performed to verify these observations.

As a first step to compare the performance of these tools, the stability limits and the material removal rates (MRR) of the solid, hollow and the damped tool were plotted together to see any difference. Figure 4-18 shows such a plot.

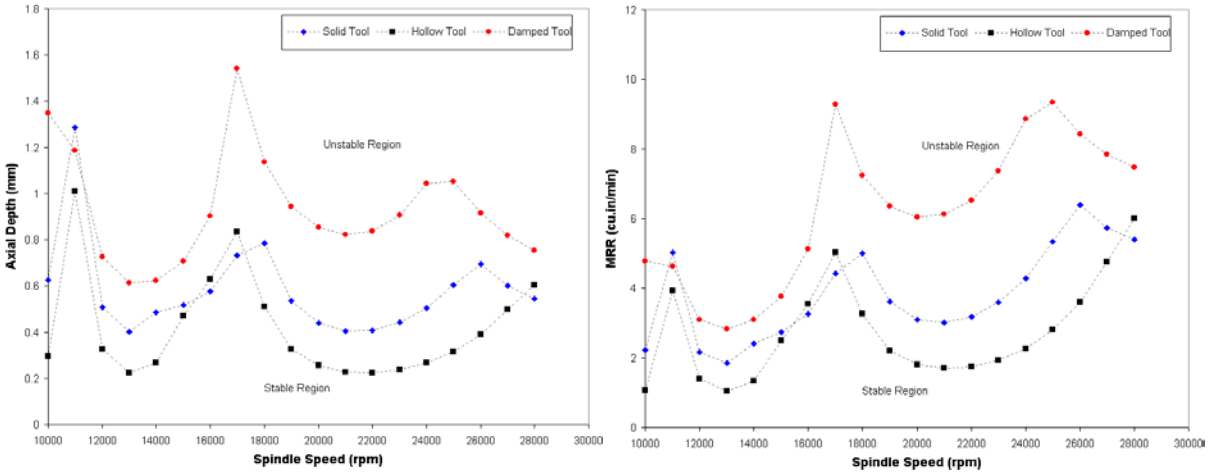

Figure 4-18. Points from stability lobes generated from static measurements (left) and corresponding MRR (right) for all the three tools.

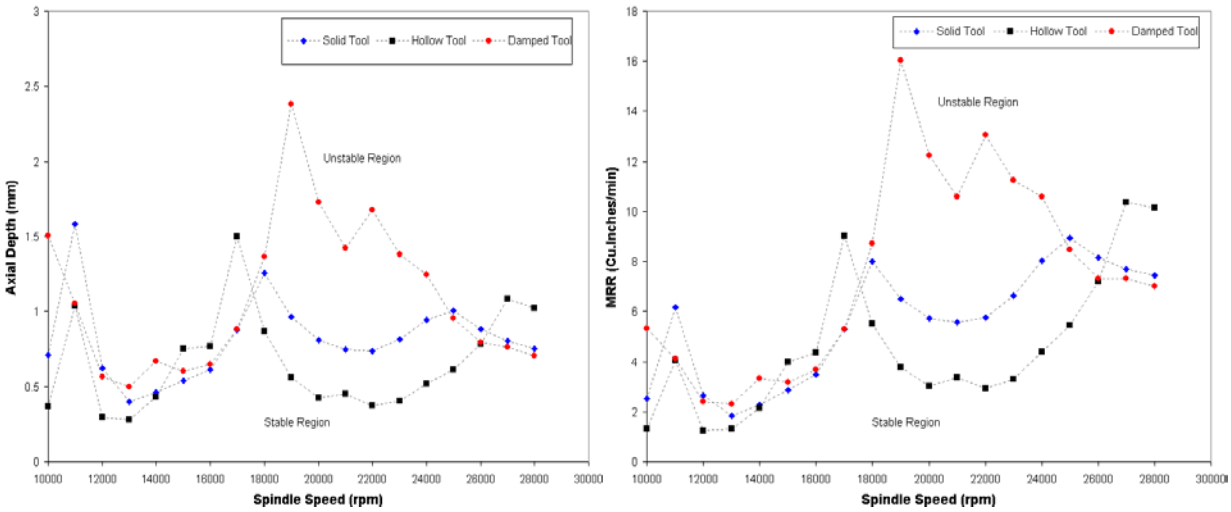

Figure 4-19. Points from stability lobes generated from different spindle speeds (left) and corresponding MRR (right) for all the three tools.

The measurements predicted that the damped tool should perform better than the solid or hollow tools. To verify these predictions, cutting tests were performed on all these tools.

CHAPTER 5
RESULTS FROM THE CUTTING TESTS

The results from the FRF measurements and the stability lobes obtained from the previous were verified through the cutting tests on the tools.

The tests were performed to verify two observations:

1. The influence of spindle speeds on the shift in the stability limits.
2. The effect of frictional damping on cutting tools.

As mentioned earlier, the tool used for the research was a high-speed steel 3-fluted end mill with the center- cutting flute, which enables it to perform slotting cuts. The tool was fabricated using the ANCA-RGX five axis tool grinder. Identical flute profiles were maintained for both solid and the hollow tool. A 3-fluted cutter was chosen based on past experience with high speed milling of aluminum.

The work piece material chosen for the cutting test was aluminum 6061, which is an alloy with the density of 2700kg/m^3 and Modulus of Elasticity of 69GPa. Care was taken in preparing the work piece to avoid any surface irregularities that might affect the accuracy in axial depths. Clamps and other fixtures were used to make sure that the work piece was held properly on the worktable of the machine.

HSM1 was built in July 1996 at the Machine Tool Research Center to demonstrate high-speed machining techniques to the manufacturing industries. It has a spindle power of 36KW and can run at a maximum speed of 36000 rpm. It can travel with a speed of up to 30 m/min in x and y directions and 15 m/min in z-direction, with an acceleration of 2g.

After preparing the tool and the work piece for the cutting tests. Programming of the tool path had to be done on HSM1. The cutting tests involved only a simple slotting routine. A chip load of 0.004 in/tooth was chosen for the tests.

The stability limit plots obtained from the previous chapter were used to guide the choice of cutting parameters in the tests. It was decided to perform the tests in the regions where there was a significant difference in predicted stability limits between the tools.

The procedure that was followed to perform the cutting tests was,

1. The tool was mounted on to the spindle with the same amount of torque that was applied while measuring the FRFs.
2. The work piece was cut, deburred and was checked for any surface irregularities before clamping securely onto the worktable of the machine.
3. The coordinates of the work piece including the z-depth were found and were included in the tool path program.
4. A slotting cut was chosen as the test routine and all the cuts were done in the x-direction.
5. A constant chip load was used for all tests. For every speed chosen, feed rate was calculated and was included in the NC program. The feed rate was calculated using the formula,

$$\textit{Feed rate} = \textit{spindle speed} \cdot \textit{chip load} \cdot \textit{number of teeth}$$

6. For every speed chosen the axial depths were incremented until the tool chattered. The cut that was made before the tool chatter was chosen to be the stable limit for the tool at that rpm.
7. The same procedures were followed in testing all the three tools.

Chatter Recognition

Identifying tool chatter while performing the cutting tests was an important issue. It is well known that chatter is a self-excited vibration and often results in undesired surface quality and reduced tool life.

Researchers in the area of high-speed milling have implemented various chatter recognition techniques. Professor Jiri Tlusty developed a method that detects chatter during machining, and in turn, suggests a new speed for the same depth. This was achieved by recording the audio signal during the cut and, later, performing a discrete Fourier transformation (FFT) of the time-based sound signal. In doing this, a plot with all the frequency contents involved during the cut can be obtained. By filtering out the tooth passing frequency and its harmonics, peaks of chatter frequencies can be recognized.

In another technique [14], tool chatter was recognized from once-per-revolution milling audio signal. This was achieved by using a microphone and a infrared emitter/detector. This method used the synchronous and asynchronous nature of stable and unstable cuts, respectively, to identify chatter. The idea was developed based on the fact that stable cuts generate content synchronous with the speed and, therefore the once-per-rev signal will be characterized by tightly placed cluster of values. On the other hand the unstable cuts would demonstrate an asynchronous motion with the speed resulting in a much-distributed data from the sensor. This technique was developed by Schmitz and used statistical evaluation to compare the variance between the stable and the unstable cuts.

Figure 5-1. A setup to perform the cutting tests with a unidirectional microphone for measuring the audio signal during the cut.

Similar to the technique developed by Professor Tlusty, a qualitative method to identify chatter, based on sound signal was developed. During the cutting process, the sound of the cut and the visual appearance of the cut surface were monitored to provide a preliminary assessment of the stability of the cut. The audio signal during the cut was also recorded using a unidirectional microphone. Following the completion of the tests, a FFT of the time based sound data was performed. The onset of chatter was verified by the appearance of a new frequency as the cut went deeper and chatter developed. This point was deemed as chatter and the identified frequency was labeled chatter frequency. This was also confirmed by closer inspection of the surface of the machined work piece.

Matlab routines were developed to perform this task. The audio signal was recorded for about 5 seconds with the sampling frequency of 22 KHz. A function called *wavrecord* was used to record the signal. One such plot taken during the cut can be seen in Figure 5-2.

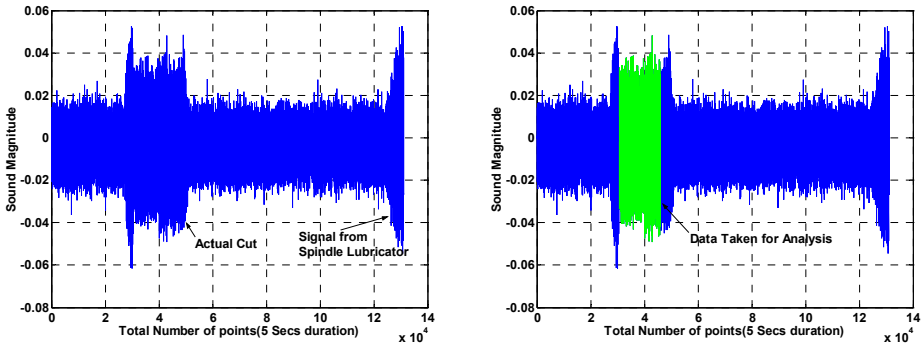

Figure 5-2. Time based sound magnitude data (left) taken for 5secs and the part of the data that would be taken for analysis (right).

The sound signal obtained has different characteristics during the cut, but also shows other noise sources such as the bearing lubricator and the air supply. Initially, to avoid any contribution to the recorded signal from an external source, the bearing lubricator was switched off during the cut and was later switched on. Only a portion of

the data during the cut was used (as shown in Figure 5-2 on the right hand side) to perform the FFT. The time based sound data was stored as a vector in an ASCII file and a subroutine for performing the Fourier transform was used to obtain the signal in the frequency domain.

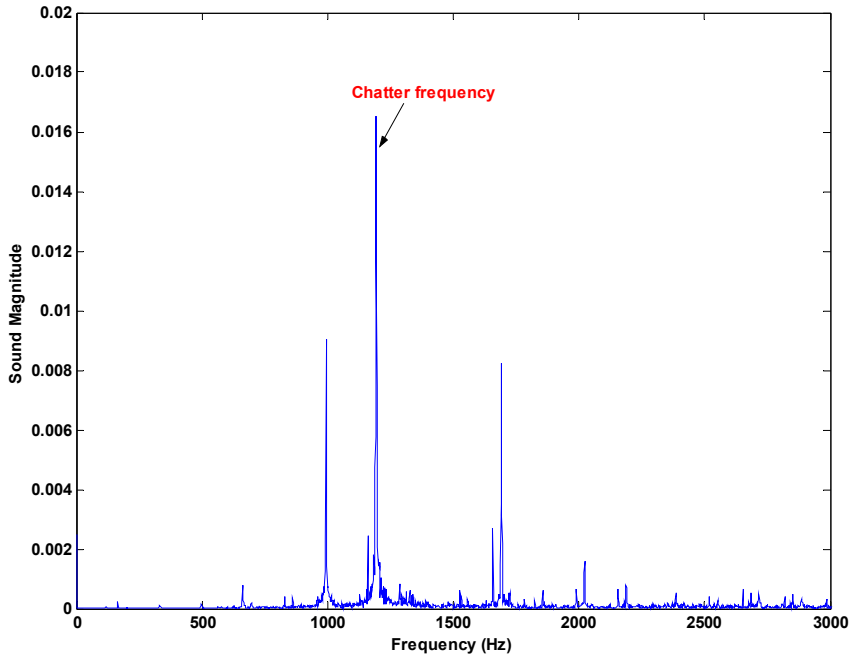

Figure 5-3. A FFT plot of the sound magnitude obtained at 10000 rpm

This method proved be quite successful in identifying the chatter frequency, and was found to have a very good agreement with the surface quality.

To illustrate more clearly, the relationship between the output of the sound signal and the surface quality, Figure 5-4 shows the result of a cutting test performed on the damped tool at 10000rpm. The tooth passing frequency at this spindle speed was 500Hz and the spindle frequency was 166Hz. The axial depth of cut was increased in steps of 0.25mm starting from 0.5mm. From the FFT plots, for depths starting from 0.5mm up to 1.5mm, the only set of frequency contents that can be seen are the tooth passing

frequency and its harmonics, this clearly shows that tool is in its stable region. Going beyond this depth, at 1.75mm the tool enters its stability limit zone and a tiny spike at 1100 Hz begins to appear. At the depth of 2mm this spike drastically increases in magnitude and establishes itself as a well-defined chatter frequency, which is roughly around the frequency of the tool mode. This change in behavior can be seen very obviously on the machined surface.

Results obtained from these tests were quite reliable, and FFT plots of the sound signal were generated for all the cutting tests performed and were later were visually verified with the surface finish.

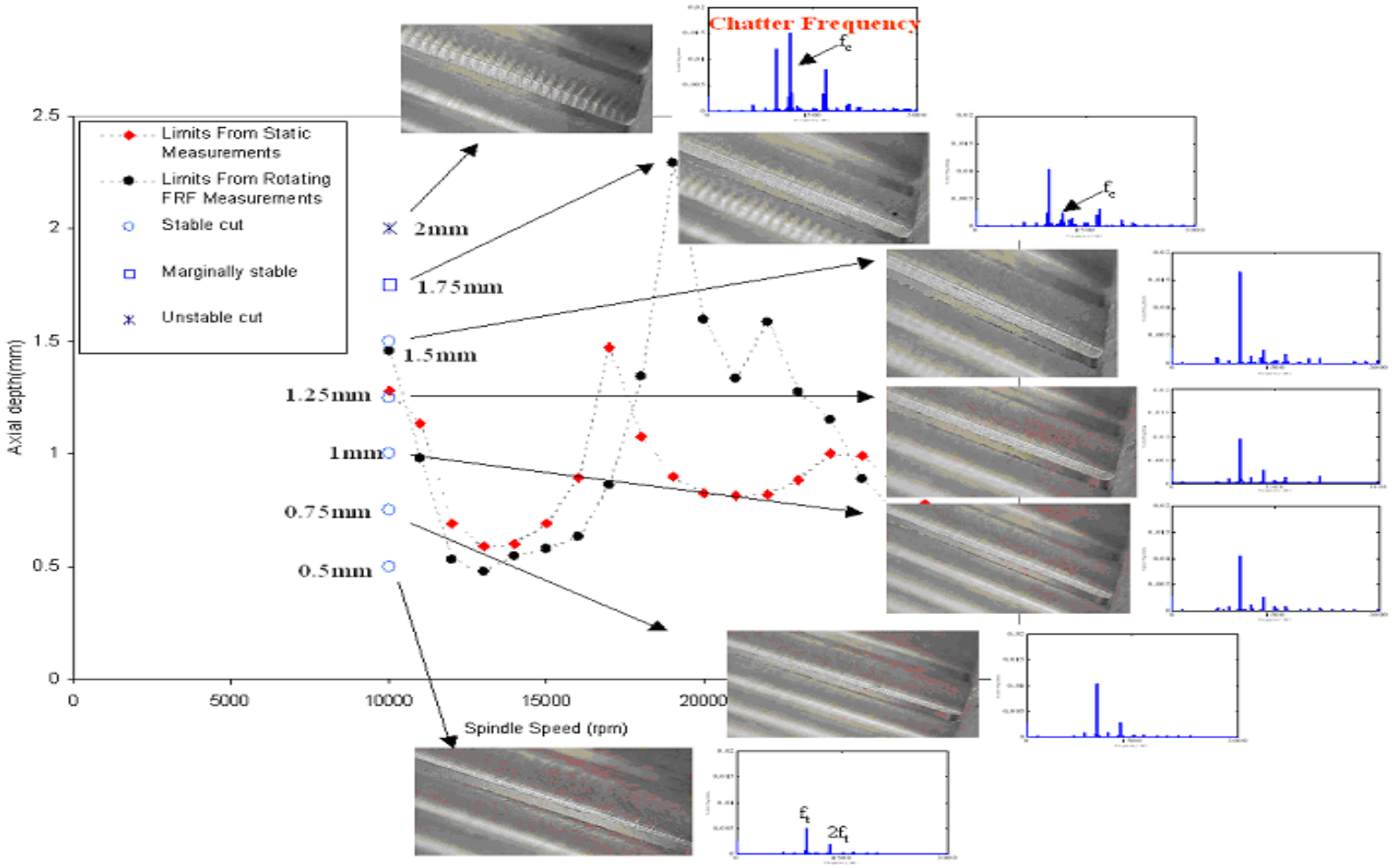

Figure 5-4. Results from the cutting tests performed at 10000rpm using a damped tool, ft is the tooth passing frequency and fc is the chatter frequency.

The cutting tests were performed on all the three tools and the stability limits were identified using the method outlined above.

The results from the cutting tests performed on the solid, hollow and the damped tool are shown below.

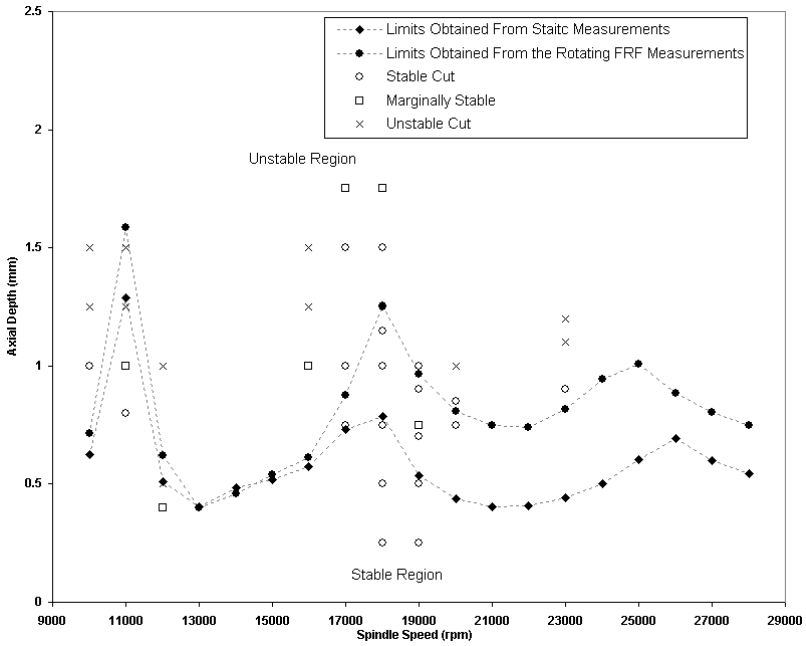

Figure 5-5. Results from cutting tests performed on the solid tool.

The results obtained from the cutting tests performed on the solid tool shows very clearly that, the stable zone lies above the stability limits predicted from the static measurements, particularly at higher speeds. The stability limits predicted from the rotating FRF measurements more closely predict the stability limit. These results show that the changing spindle dynamics with speed had a significant effect of the stability limit. The same trend was observed with the hollow and the damped tool.

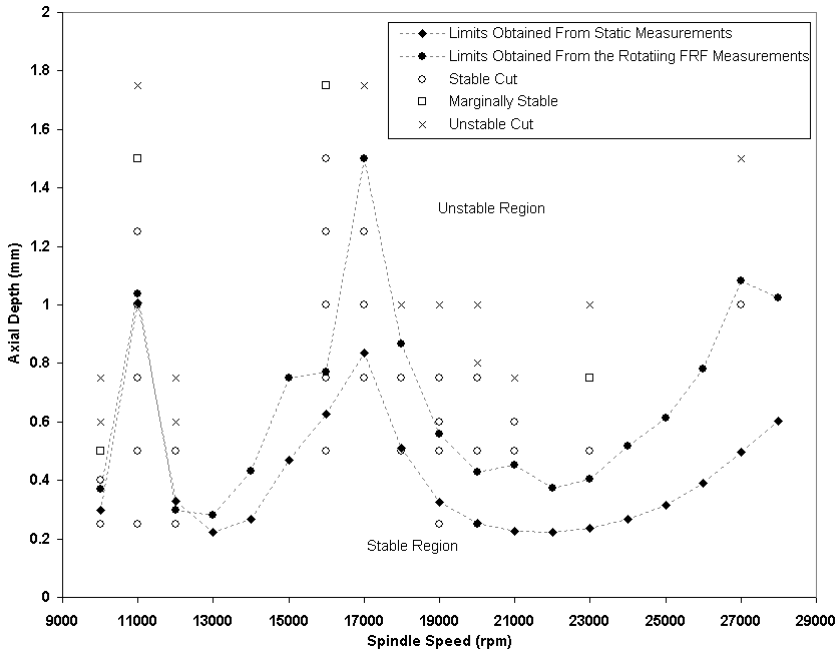

Figure 5-6. Results from the cutting tests performed on the hollow tool.

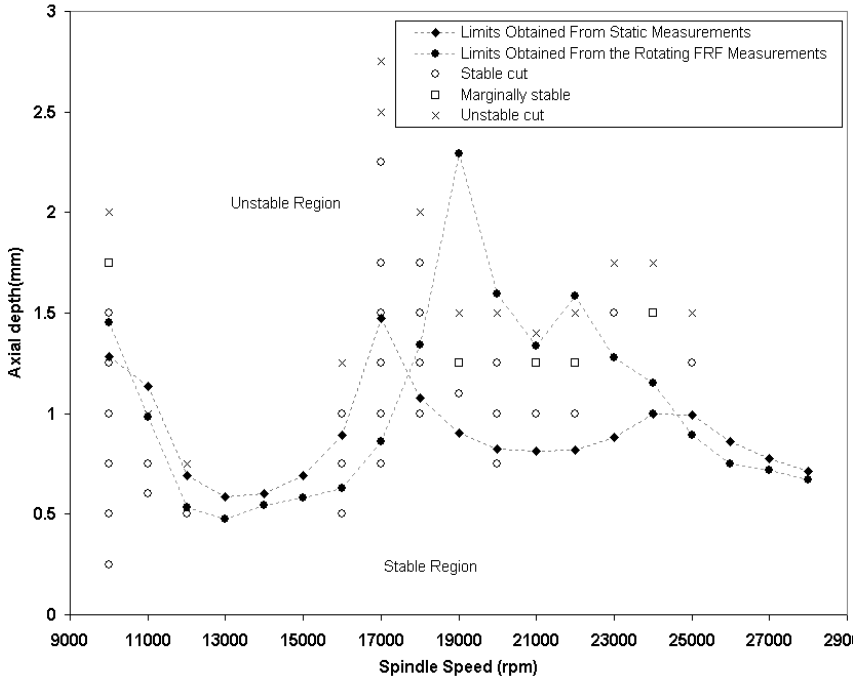

Figure 5-7. Results from the cutting tests performed on the damped tool.

Notice that some of the points from the actual measurements are slightly deviated from the stability limit values obtained from rotating FRF measurements. This may be due to the choice of cutting coefficients values used to generate the stability lobes. The values chosen for these tests were typical and may not have reflected the exact properties of the work piece material and tool geometry used for this research.

This achieves the first objective of the cutting tests, confirming that the spindle speed, indeed, affects the dynamic characteristics of the cutting tool.

Effect of Frictional Damping

Figure 5-8 compares the stability limit vs. speed for the 3 tools tested to examine the effect of the centrifugal damper.

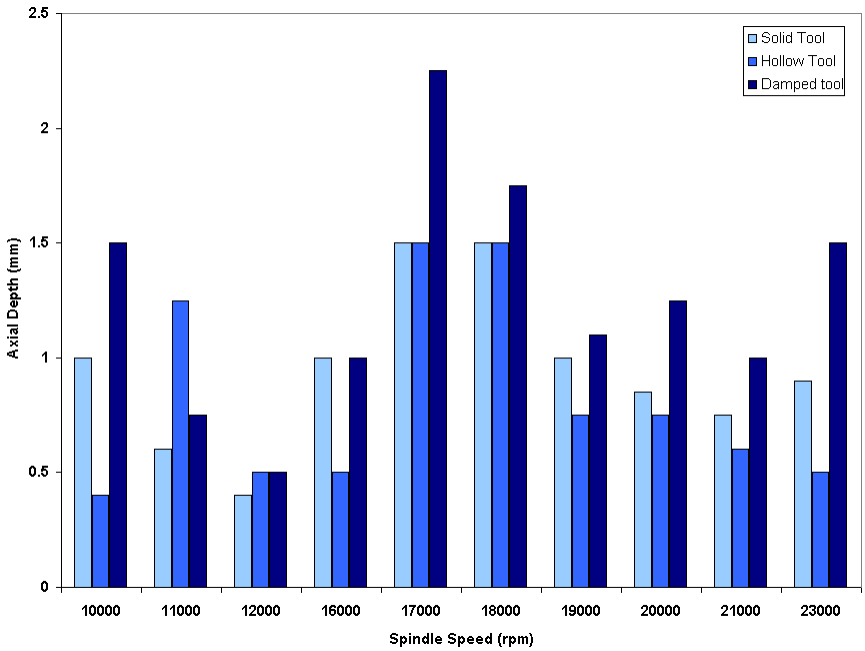

Figure 5-8. Actual depth of cut achieved on all the three tools.

The figure clearly shows that in almost all the speeds the damped tool has outperformed both the solid and the hollow tool. Plots showing the percentage of improvement exhibited by the damped tool at these speeds are given below.

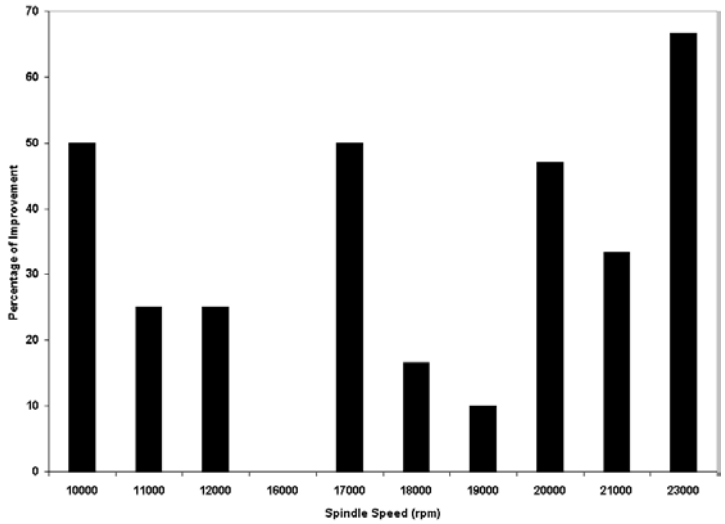

Figure 5.9 Percentage of improvement in cutting depths when compared with the solid tool.

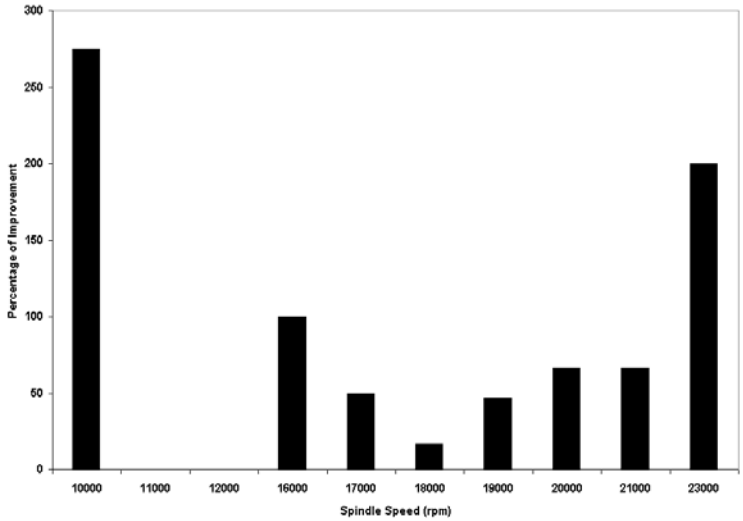

Figure 5-10 Percentage of improvement in cutting depths when compared with the hollow tool.

It can be seen that the damped tool performed very well at higher speeds than a solid tool exhibiting the effect of frictional damping. A maximum improvement of 66% in cutting depth was achieved at around 23000 rpm over the solid tool and an improvement of 275% in cutting depth was achieved at around 10000 rpm over the hollow tool. Notice that there was no improvement on the damped tool at the speed of

16000 rpm when compared with the solid tool, and also at the speed of 11000 rpm and 12000 rpm over the hollow tool. This is likely due to the shift in natural frequency of the tools due to their different masses. A change in natural frequency of the tool moves the lobes either to the left or right on the lobing diagram may shift the optimal spindle speeds for maximum stability for that tool. Another reason would be because of competing lobes. When developing lobes from multi-degrees of freedom systems, there are always more than one set of lobes, and when these lobes cross over each other in a region, they tend to cut the stability limits and result in bringing them to a lower value.

CHAPTER 6
CONCLUSIONS AND RECOMMENDATIONS FOR FUTURE WORK

The research work was started with an objective to increase the material removal rate (MRR) by improving the dynamic stability of endmills. A frictional damper model was introduced and the idea behind the proposed model was explained.

Two theoretical models were presented and the equations to calculate the frictional work were derived. Also, the work magnitudes were calculated for all possible finger configurations to optimize the design.

A description of the tool selected for the research was given along with its material properties.

The instrumentation and the initial testing procedure to obtain the FRFs were described. Later, observations made on the change in tool characteristics during spindle rotations were verified by measuring the rotating FRFs, and stability lobes were generated from the measurements.

Three tools namely the solid, hollow, and the damped tools were used to verify this observation. Over one hundred cutting tests were performed. A method to identify chatter was introduced and the results obtained from this method were verified by inspecting the quality of the machined surface.

The cutting tests were performed on all the three tools to see the effect of frictional damping on them as well as to see the influence of spindle speeds on their predicted stability limits.

Conclusions

From the results obtained, it was found that the damped tool outperformed both the solid and the hollow tool. Although the overall performance of the damped tool was better compared to the solid tool and hollow tool, the results were exceptional when the damped tool went 66% deeper than the solid tool at 23000 rpm (1.5mm vs 0.9mm) and did four times better than the hollow tool at 10000 rpm (1.5mm vs 0.4mm). On the whole, the idea of introducing frictional damping in cutting tools was proved to be quite successful.

It was also confirmed from the cutting tests, that, the stability limits obtained from the rotating FRF measurements tends to reflect a more realistic behavior of the tool than the static measurements. These were verified by plotting the actual depths along with the stability limits predicted from the rotating FRF measurements.

The method to analyze the sound magnitude in frequency domain to identify the chatter frequency during machining was quite successful, although, a lot of improvements have to be made to refine the data acquiring technique.

Recommendations For Future Work

Given below are some recommendations that could be followed for future research.

1. The frictional damping idea, which was successful on the research tool, can be applied on a commercially available tool, and later, tests can be done to verify whether it can be recommended for mass production.

2. More research can be done to choose an alternate material for the damper to reduce the cost of fabrication.

3. Techniques such as introducing a polymer or filling the hollow tool with a visoelastic material can be tried to see any improvements.

4. The method to measure the rotating FRFs can be simplified by identifying the ranges of spindle speed where the tool's response would remain fairly constant. By doing this, a complete set of stability limits can be obtained for the entire working

range of the spindle without spending time on measuring them in small and discrete steps.

5. Research work can be done to design spindles that exhibit change in dynamic behavior at higher speeds.

6. Although the simple chatter recognition technique adopted was quite useful, the signals obtained from these measurements were quite noisy. A more refined method of measuring the sound signal can be introduced, such as, using a once per revolution sensor to identify the exact spindle speed and later this feedback can be used to eliminate the known frequency contents and display only the chatter frequency.

Overall, the research work initiated an effort to improve the quality of the existing cutting tools and introduced a way to improve productivity in high-speed machining.

APPENDIX A
ADDITIONAL MATHEMATICAL DERIVATIONS

The frictional work calculation derived in Chapter 3 involves variables such as the moment of inertia I_f of the fingers and I_t of the tool, the distance d between the neutral axis of the finger and the neutral axis of the beam, the volume, and the contact force P. A derivation for these variables will be presented for both the geometrical designs.

Damper made of carbide

These derivations were already done by Sterling using MathCAD. The variable I_{fi} is the moment of inertia of the *i*th finger in the composite structure. It is itself made up of variables consisting of its own geometric parameters. The expression for I_{fi} must be made up of these simpler variables in order to make the entire work function a function of a few simple parameters. With this in mind, a expression for the moment of inertia was developed by considering the circular sector of Figure 3.1.

From the figure, r_1 is the inside radius and r_2 is the outside radius of the sector. Theta is measured counter-clockwise from the horizontal as shown, and dr is a differential arc element of the sector. The moment of inertia of any point about the x-axis is given by

$$I_x = \int y^2 \, dA$$

The y-distance from the neutral axis to any point on the sector can be written as

$$y = r \cdot \sin(\theta)$$

The differential area of the element at this point is

$$dA = dr \cdot d\theta \cdot r$$

Substituting these into the inertia moment equation,

$$I_x = \int_{\theta_1}^{\theta_2} \int_{r_1}^{r_2} r^3 \cdot (\sin(\theta))^2 \, dr \, d\theta$$

Integrating this, we get a function of four variables of the form

$$I_x(r_1, r_2, \theta_1, \theta_2) = \frac{1}{8} \cdot \begin{pmatrix} -r_2^4 \cdot \cos(\theta_2) \cdot \sin(\theta_2) + r_2^4 \cdot \theta_2 + r_1^4 \cdot \cos(\theta_2) \cdot \sin(\theta_2) - r_1^4 \cdot \theta_2 \ldots \\ + r_2^4 \cdot \cos(\theta_1) \cdot \sin(\theta_1) - r_2^4 \cdot \theta_1 - r_1^4 \cdot \cos(\theta_1) \cdot \sin(\theta_1) + r_1^4 \cdot \theta_1 \end{pmatrix}$$

This is the moment of inertia about the x-axis of any annular finger in any orientation with any inside and outside radius. Since the model assumes a force in the y-direction, it is acceptable to use this moment in the model. The variables r_1 and r_2 represent the inside and outside radii of the finger in question. The variables θ_1 and θ_2 represent the starting and ending angles (relative to a zero-direction corresponding to the positive x-axis) of the cross section of the finger. Assuming that all fingers in the structure have equal radii, this equation is used for each finger with θ_1 and θ_2 being different for each.

The variable d is the y-distance between the neutral axes of any finger in any position to the neutral axis of the entire structure (which lies along the neutral axis of the outer member, the tool shank). Taking the neutral axis of the structure to be the zero point, d can be analyzed as follows.

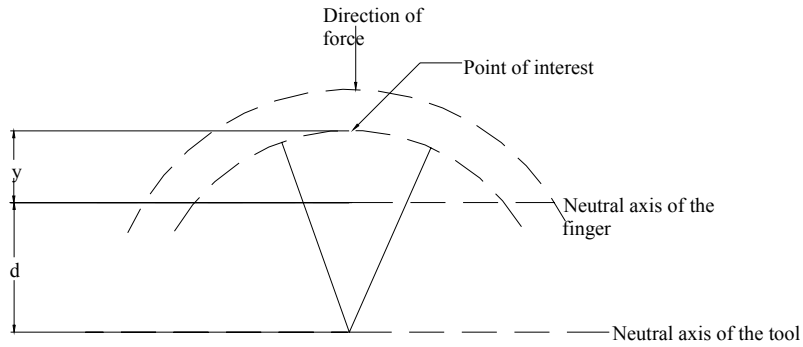

Figure A-1. The references of a point on the surface of a finger.

The first moment of area about the x-axis of any two-dimensional shape is

$$Q_x = \int y \, dA$$

The above expressions for y and dA in terms of r and θ can be plugged into the equation for first moment of area, again using a double integral for the two variables. Doing this and performing the integration,

$$Q_x = \int_{\theta_1}^{\theta_2} \int_{r_1}^{r_2} r^2 \cdot \sin(\theta) \, dr \, d\theta$$

$$Qx = \frac{-1}{3} \cdot \cos(\theta_2) \cdot r_2^{\,3} + \frac{1}{3} \cdot \cos(\theta_2) \cdot r_1^{\,3} + \frac{1}{3} \cdot \cos(\theta_1) \cdot r_2^{\,3} - \frac{1}{3} \cdot \cos(\theta_1) \cdot r_1^{\,3}$$

This is the expression for the area moment of inertia for an annular sector. The centroid of a shape is the area moment of inertia divided by the area of the shape. In this case, using the variables of the established notation, the area is

$$\text{Area} = \frac{(\theta_2 - \theta_1) \cdot (r_2^{\,2} - r_1^{\,2})}{2}$$

If the area moment is divided by the area, the result is

$$y_{bar} = \frac{2\cdot\left(\frac{-1}{3}\cdot\cos(\theta_2)\cdot r_2^3 + \frac{1}{3}\cdot\cos(\theta_2)\cdot r_1^3 + \frac{1}{3}\cdot\cos(\theta_1)\cdot r_2^3 - \frac{1}{3}\cdot\cos(\theta_1)\cdot r_1^3\right)}{\left[(\theta_2 - \theta_1)\cdot\left(r_2^2 - r_1^2\right)\right]}$$

Again, this is the y-distance from the neutral axis of the finger to the neutral axis of the structure in terms of r_1, r_2, θ_1, and θ_2.

For the pressure of the inside member on the outside member, we can take the centripetal force on the inside member. Treating it as a beam, it has a volume of,

$$\text{Volume}(\theta_1, \theta_2, r_1, r_2, \text{Length}) := \left(\frac{\theta_2 - \theta_1}{2}\right)\cdot\left(r_2^2 - r_1^2\right)\cdot\text{Length}$$

The mass is the volume times the density. The radius at which this mass is centered is the distance, d, defined above. The centripetal force on the member is then

$$F_c = \text{Volume}\,\rho\cdot\omega^2\cdot d$$

The pressure that this force produces is given by

$$P = \frac{F_c}{\text{Length}\cdot(\theta_2 - \theta_1)\cdot r_2} = \frac{\text{Volume}\,\rho\cdot\omega^2\cdot d}{\text{Length}\cdot(\theta_2 - \theta_1)\cdot r_2}$$

Writing this in a useable form,

$$P(\theta_1, \theta_2, r_1, r_2, \text{Length}, \omega, \rho) = \frac{\text{Volume}(\theta_1, \theta_2, r_1, r_2, \text{Length})\cdot\rho\cdot\omega^2\cdot d(r_1, r_2, \theta_1, \theta_2)}{\text{Length}\cdot(\theta_2 - \theta_1)\cdot r_2}$$

Damper Made Of Stainless Steel

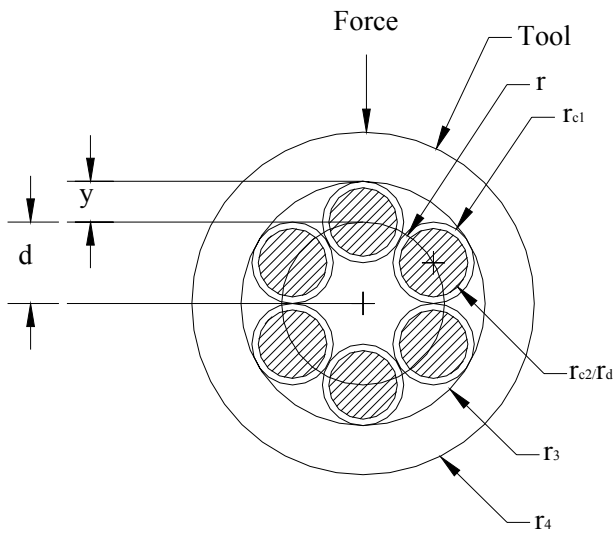

r_4 = outer radius of the tool
r_3 = inner radius of the tool
r_{c1} = inner radius of the sleeve
r_{c2} = outer radius of the sleeve
r_d = radius of the finger
r = radial distance from the center of the tool to the center of the finger or rod

Figure A2 Sectional view of the modified design.

The moment of inertia of the finger is given by,

$$I_f = \frac{r_d^{\,4}\pi}{4} + \left(r_d^{\,2}\pi\left(r^2\left(\sin(\theta)\right)^2\right)\right)$$

and the tool,

$$I_{tool} = \frac{\left(r_4^{\,4} - r_3^{\,4}\right)\pi}{4}$$

The distance between the neutral axis of the finger and the neutral of the tool measured with respect to y-axis of the tool is given by the formula,

$d = r\sin\theta$

The volume of the damper is given by,

Volume= volume of the fingers + volume of the sleeves

Therefore,

Volume = $\pi \cdot r_d^2 \cdot$length of the finger or rod + $\pi \cdot (r_{c2}^2 - r_{c1}^2) \cdot$length of the sleeve

The centrifugal force due to the spindle rotation where the fingers thrust against the inner surface of the tool is given by,

$$\text{Cforce} = \frac{\text{Volume} \cdot \text{density} \cdot (\text{spindle speed} \cdot 2\pi)^2 \cdot \text{r}}{2}$$

The values obtained from these formulas were later used in the frictional work calculations.

APPENDIX B
MATLAB CODES

The Matlab code to calculate the frictional work done by the original damper design is given below.

```
%TO FIND THE FRICTIONAL WORK DONE BY THE DAMPER (S.I UNITS)
clear all;
close all;
strtang=45*pi/180;                    %STARTING ANGLE(RAD)
f=14;                                 %CALCULATING WORK FOR A DAMPER UPTO 14 FINGER
CONFIGURATION
for n=2:                              %NUMBER OF FINGERS
    o(n)=n+1;
    theta(1)=strtang;
    fingang=2*pi/n;                   %ANGLE MADE BY EACH FINGER
    for i=2:n+1
    theta(i)=theta(i-1)+fingang;
    end
%%%%%%%%%%%%%%MATERIAL PROPERTIES%%%%%%%%%%%%%
E1=2.06799994879999998e11;        %YOUNG'S MODULUS OF TOOL (Pa)
E2=2.06799994879999998e11;        %YOUNG'S MODULUS OF DAMPER (Pa)
ro=7.82e3;                        %DENSITY OF THE MATERIAL (Kg/m^3)
mu=0.15;                          %COEFFICIENT OF FRICTION
%%%%%%%%%%%%%%%%%%%GEOMETRY%%%%%%%%%%%%%%%%%%
L=114.16e-3;                              %TOTAL LENGTH OF THE DAMPER(m)
r2=4.7625e-3;                             %OUTER RADIUS OF THE DAMPER(m)
r3=r2;                            %INNER RADIUS OF THE TOOL(m)
r1=1.5e-3;                        %INNER RADIUS OF THE DAMPER(m)
r4=9.525e-3;                              %OUTER RADIUS OF THE TOOL(m)
%DYNAMICS
omega=433;                                %SPEED OF THE TOOL IN RPS
force=100;                                %VERTICAL FORCE (N)
%%TO CALCULATE THE SUM OF MOMENT OF INERTIA OF THE INNER AND OUTER
MEMBERS%%
    I_finger=0;
    w=0;
    I_tool=1/4*pi*((r4^4-r3^4));
    for i=1:n
    n1(i)=i;
    u=1/8*((r1^4-r2^4)*((cos(theta(i+1)*sin(theta(i+1)))-(cos(theta(i))*sin(theta(i))))-(theta(i+1)-
theta(i))));
    I_finger=I_finger+u;
    EIsum(i,n)=I_tool*E1+I_finger*E2;
    end
%%%%%%%%%%FRICTION WORK CALCULATION%%%%%%%%%%
    for i=1:n
    n1(i)=i;
    d(i,n)=(2*(cos(theta(i+1))-cos(theta(i)))*(r1^3-r2^3))/(3*(theta(i+1)-theta(i))*(r2^2-r1^2));
    vol(i,n)=((theta(i+1)-theta(i))/2)*(r2^2-r1^2)*L;
    centri_f(i,n)=(vol(i,n)*ro*(omega*2*pi)^2*d(i,n))/(sin((theta(i)+theta(i+1))*0.5)*L)
```

```
%%%%%%%%%%%%%%%FINALWORK CALCULATION FOR INDIVIDUAL
FINGERS%%%%%%%%%%%%%%
    work(i,n)=-(L^3*mu*centri_f(i,n)*force*d(i,n))/(3*EIsum(i,n));
    w=w+abs(work(i,n));
    y=w;
    end
    b(n)=y;
    y=0;
```

Second Design

The frictional work calculation for the second design is given below

```
%TO FIND THE WORK DONE BY THE SECOND DAMPER (S.I UNITS)
clear all;
close all;
strtang=45*pi/180;              %STARTING ANGLE(RAD)
f=14;                       %CALCULATING WORK FOR A DAMPER UPTO 14 FINGER
CONFIGURATION
for n=2:                     %NUMBER OF FINGERS
   o(n)=n+1;
   theta(1)=strtang;
   fingang=2*pi/n;             %ANGLE MADE BY EACH FINGER
   for i=2:n+1
   theta(i)=theta(i-1)+fingang;
   end
%%%%%%%%%%%%%%MATERIAL PROPERTIES%%%%%%%%%%%%%
E1=2.06799994879999998e11;        %YOUNG'S MODULUS OF TOOL (Pa)
E2=2.06799994879999998e11;        %YOUNG'S MODULUS OF DAMPER (Pa)
ro=7.82e3;                    %DENSITY OF THE MATERIAL (Kg/m^3)
mu=0.15;                      %COEFFICIENT OF FRICTION
%GEOMETRY
L=114e-3;                     %FULL LENGTH OF THE DAMPER(m)
Lbase=10.10e-3;                  %LENGTH OF THE BASE (m)
Lcollar=10e-3;                  %LENGTH OF THE SLEEVE (m)
rb1=0;
r4=9.52e-3;                   %OUTER RADIUS OF THE TOOL
r3=4.725e-3;                   %INNER RADIUS OF THE TOOL
%DYNAMICS
omega=433;                     %SPEED OF THE TOOL IN RPS
force=100;                    %VERTICAL FORCE (N)
%TO CALCULATE THE SUM OF MOMENT OF INERTIA OF THE INNER AND OUTER MEMBERS
I_finger=0;
w=0;
ri=4.7625e-3;
rc1=ri*(sin(fingang/2))/(1+sin(fingang/2));
rcen=ri-rc1;
rd=rc1-0.25e-3;
rc2=rd;
I_tool=1/4*pi*((r4^4-r3^4));
   for i=1:n
   n1(i)=i;
   u=((pi*rd^4/4)+(pi*rd^2*(rcen^2*(sin(theta(i)))^2)));
   I_finger=I_finger+u;
   EIsum(i,n)=I_tool*E1+I_finger*E2;
   end
%FRICTIONAL WORK CALCULATION
   for i=1:n
   n1(i)=i;
```

```
   d(i,n)=rcen*sin(theta(i));
   vol(i,n)=(pi*rd^2*L)+(pi*(rc2^2-rc1^2)*Lcollar);
   contactforce(i,n)=vol(i,n)*ro*(omega*2*pi)^2*rcen/2;
   work(i,n)=-(L^2*mu*contactforce(i,n)*force*d(i,n))/(2*EIsum(i,n));
   w=w+abs(work(i,n));
   y=w;
   end
   b(n)=y;
   y=0;
end
Matlab Code To Plot And Generate FRFs
clear all;
close all;
% Input Conversion Units, Sensitivity of Hammer, Vibrometer, and Amplifiers
   cap_sen = 2.5e-5;                          % m per Volt
   Hammer_convert = (1/2.19)*1000;                    % N/mV to N/V serial# 5960
   Amplifier_convert = 1 ;                        % 1 mV/mV
   Hammer_convert_f = Hammer_convert * Amplifier_convert;  % N/V
% LOADING THE ASCII FILE
   load filename.asc;                         % ASCII hata file composed of 3 columns - frequency, real
part, and imag part
   afrequency1 = filename(:,1);                       % Read in direct FRF data for mandrel
   areal_part1 = filename(:,2);
   aimag_part1 = filename(:,3);

   frequency1 = afrequency1;
   real_part1 = areal_part1;
   imag_part1 = aimag_part1;

   aimag_part_mod1 = aimag_part1 * (cap_sen/Hammer_convert_f); % CHANGE TO m/N
   areal_part_mod1 = areal_part1 * (cap_sen/Hammer_convert_f); % CHANGE TO m/N
   magnitude1=sqrt(areal_part_mod1.^2+aimag_part_mod1.^2);
%TO GENERATE THE FRF FROM THE APROXIMATE VALUES OBTAINED FOMR THE ASCII
FILE FOR TWO DEGREES OF FREEDOM SYATEM
natfrx1=VALUES;             %NATURAL FREQUENCY (Hz)
zetax1 = VALUES;
kx1 =VALUES;                %STIFFNESS (N/m)
wnx1 =natfrx1*2*pi ;        %OMEGA (rad/s)

natfrx2=VALUES;             %NATURAL FREQUENCY (Hz)
zetax2 = VALUES;
kx2 =VALUES;                %STIFFNESS (N/m)
wnx2 =natfrx2*2*pi ;        %OMEGA (rad/s)
%%%%%%%%%%%%%%%%%%GENERATED FRF%%%%%%%%%%%%%%%%
     frx = 8:8:6408;
     num = (frx-8);
     u = 2 * pi * num;
     GX=(((wnx1^2/kx1)./(wnx1^2-u.^2+i*2*zetax1*wnx1.*u))+((wnx2^2/kx2)./(wnx2^2-
u.^2+i*2*zetax2*wnx2.*u));
     rex = real(GX);
     imx= imag(GX);
     mag=sqrt(rex.^2+imx.^2);
%PLOT%
figure(1);
subplot(211);
plot(afrequency1, areal_part_mod1,frx,rex,'r','linewidth',1.5)
```

```
title('tool tip X-direction 17k')
xlabel('frequency, Hertz')
ylabel('Real, m/N')
legend('at the tip','below the flutes')
grid;
axis([50 5000 -1.5e-6 1e-6]);

subplot(212);
plot(afrequency1, aimag_part_mod1,frx,imx,'r','linewidth',1.5)
xlabel('frequency, Hertz')
ylabel('Imaginary, m/N')
grid;
axis([50 5000 -2.7e-6 .3e-6]);
```

Matlab Code To Record The Audio Signal During The Cut

```
%This code Records Audio signal during the cut for about 3 seconds
%Fs=Sampling Frequency
%131072 represnts total number of points for 5 seconds data(2^n(17) points)
clear all;
close all;
Fs = 22050;
y = wavrecord(131072,Fs);
matrix=[y];
save('26k_nocut.asc','matrix','-ascii')
[mag,f]=spec(y,22050);  %Calls a Subroutine to do the FFT
soundmag=abs(mag);
figure(1)
plot(f,soundmag)
axis([0 10000 0 .08])
xlabel('Frequency (Hz)');
ylabel('Sound Magnitude');
grid
```

APPENDIX C
CAD DRAWINGS OF THE DAMPER

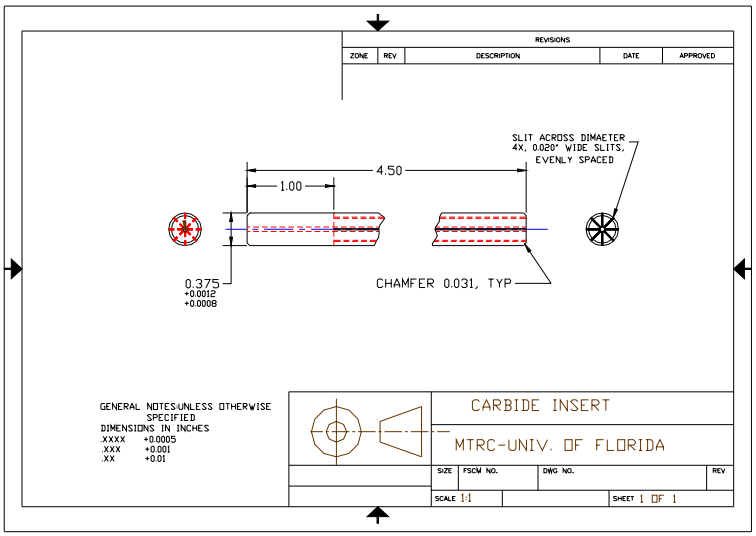

Figure C-1. Cad drawing for the original damper made of carbide.

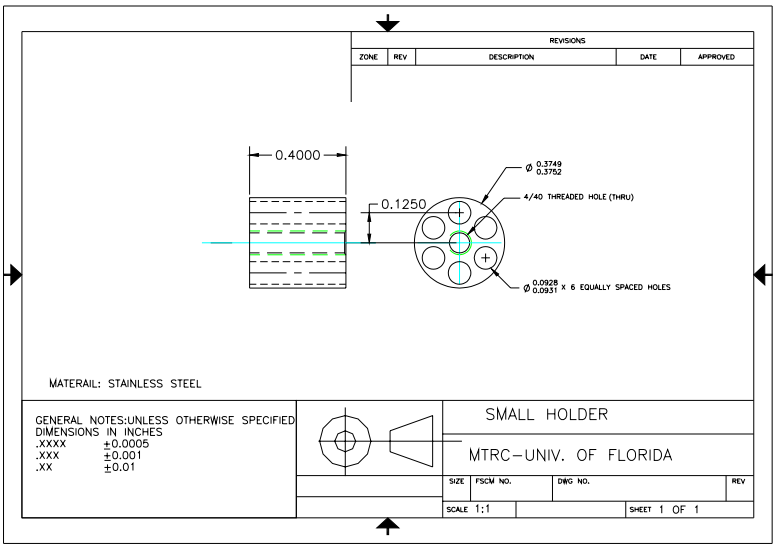

Figure C-2. Cad drawing of the second damper design showing the details of the holder or base.

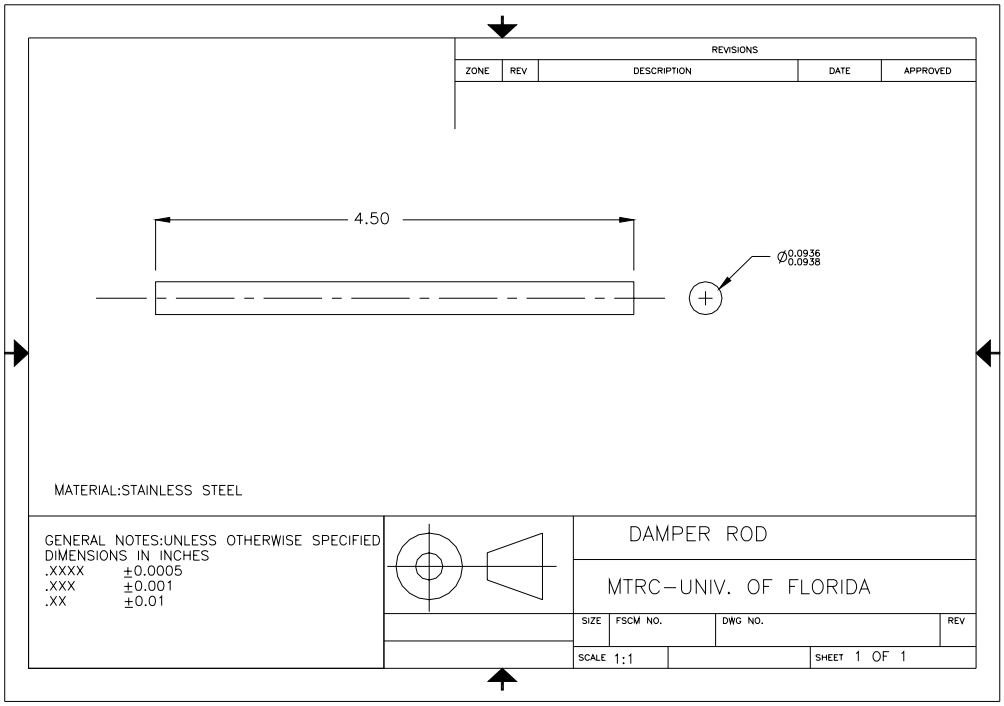

Figure C-3. Cad drawing of the second damper design showing the details of the rod.

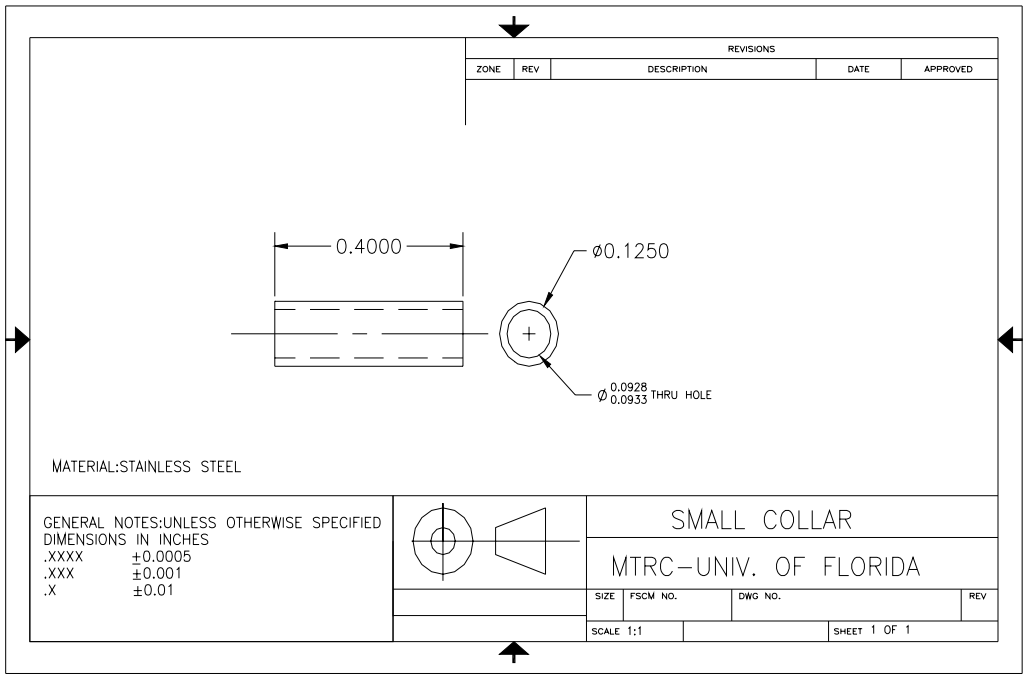

Figure C-4. Cad drawing of the second damper design showing the details of the collar.

APPENDIX D
FRF OF THE THREE TOOLS

The plots presented in this appendix are only for speeds chosen for the cutting tests.

Solid Tool

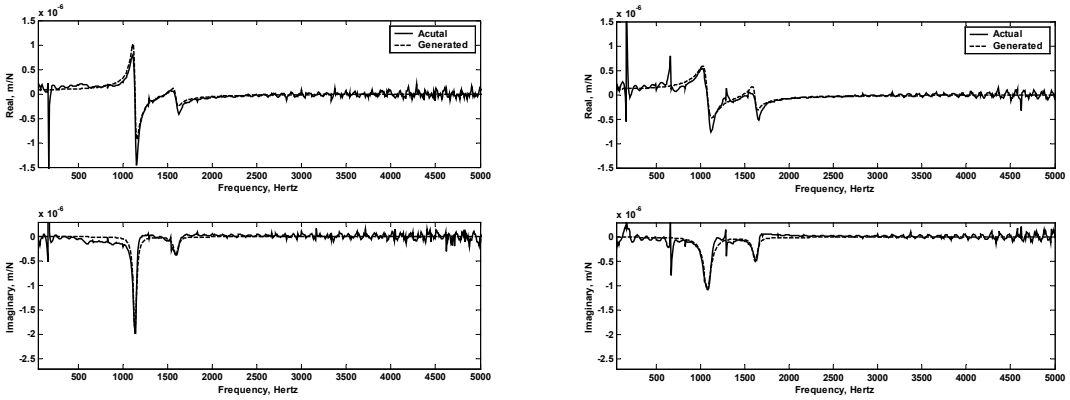

Figure D-1. FRF of the solid tool at 10000 rpm in x (left) and y (right) directions.

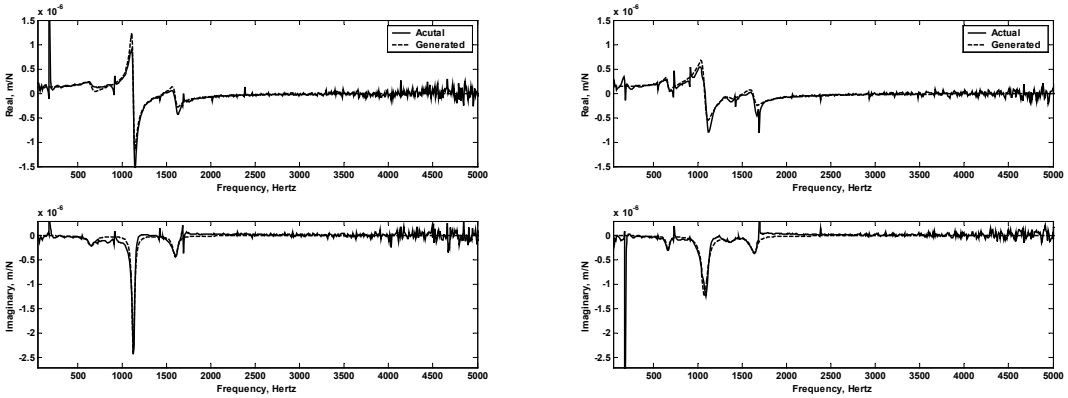

Figure D-2. FRF of the solid tool at 11000 rpm in x (left) and y (right) directions.

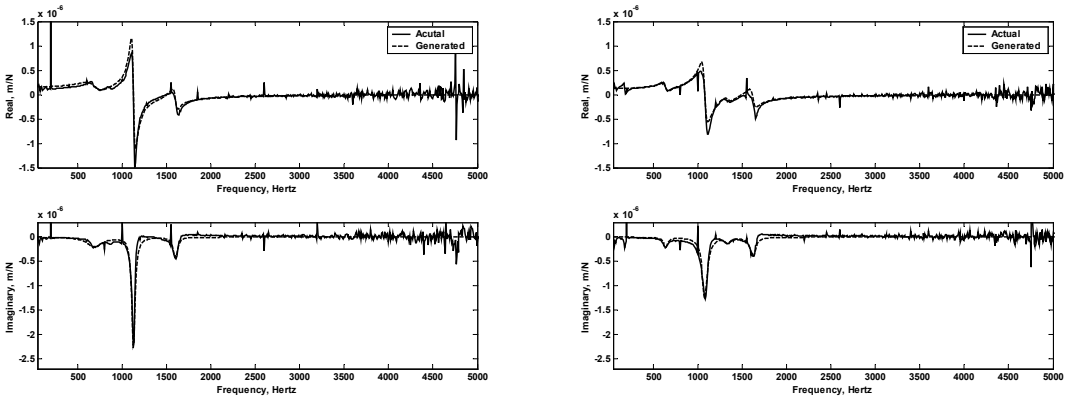

Figure D-3. FRF of the solid tool at 12000 rpm in x (left) and y (right) directions.

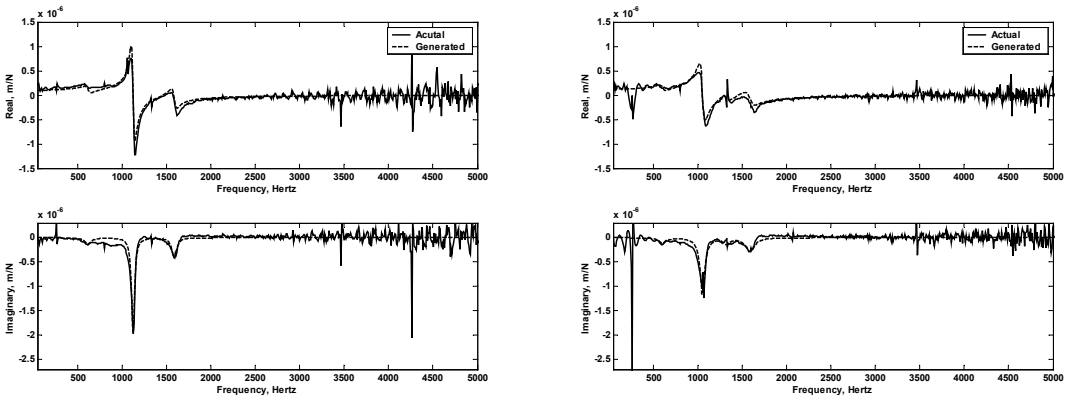

Figure D-4. FRF of the solid tool at 16000 rpm in x (left) and y (right) directions.

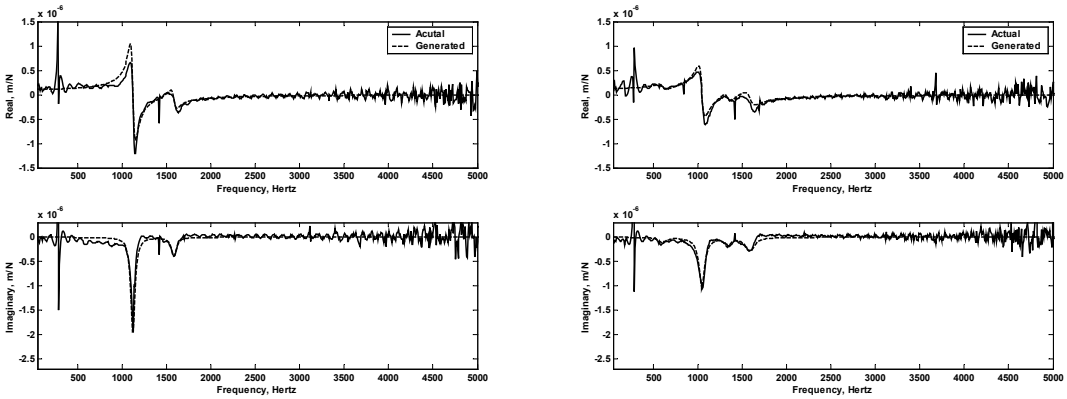

Figure D-5. FRF of the solid tool at 17000 rpm in x (left) and y (right) directions.

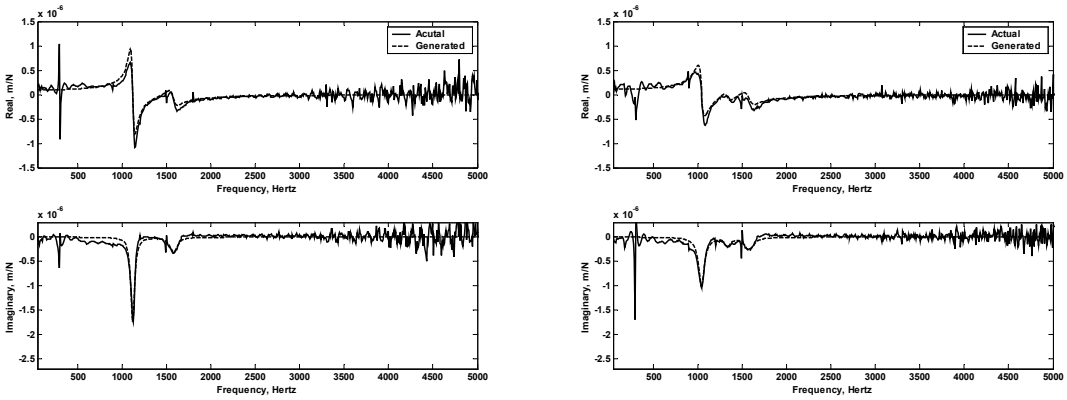

Figure D-6. FRF of the solid tool at 18000 rpm in x (left) and y (right) directions.

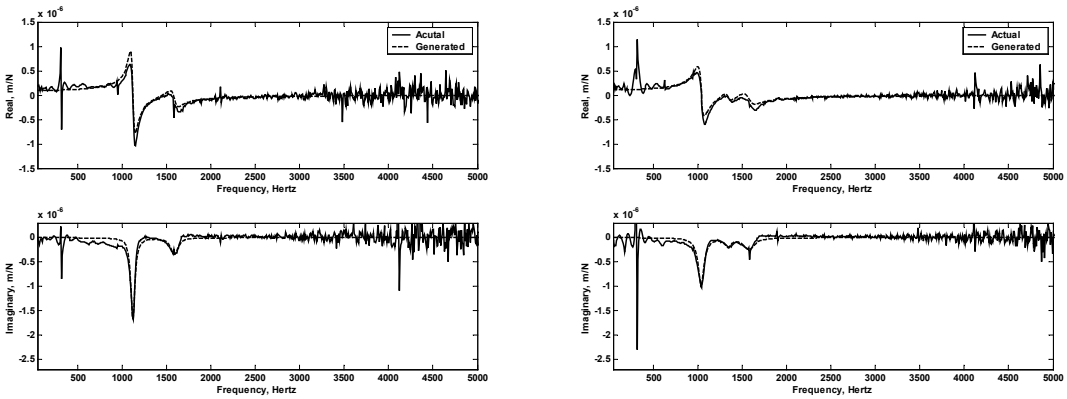

Figure D-7. FRF of the solid tool at 19000 rpm in x (left) and y (right) directions.

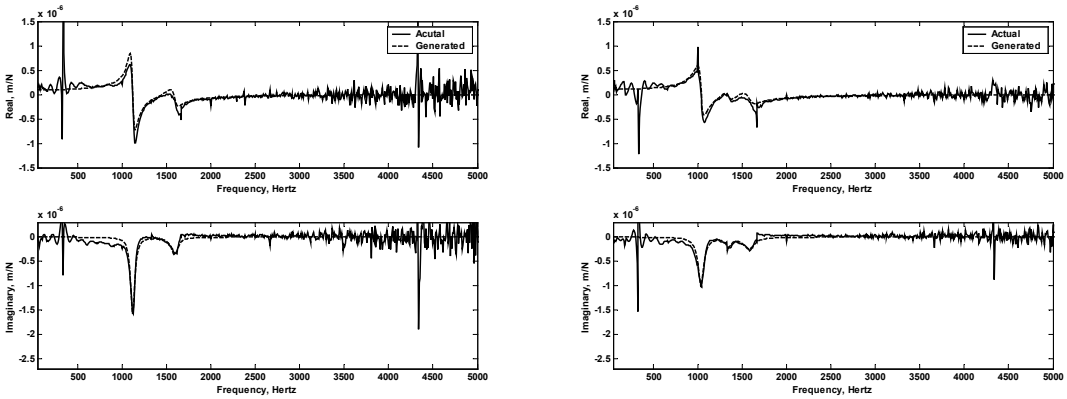

Figure D-8. FRF of the solid tool at 20000 rpm in x (left) and y (right) directions.

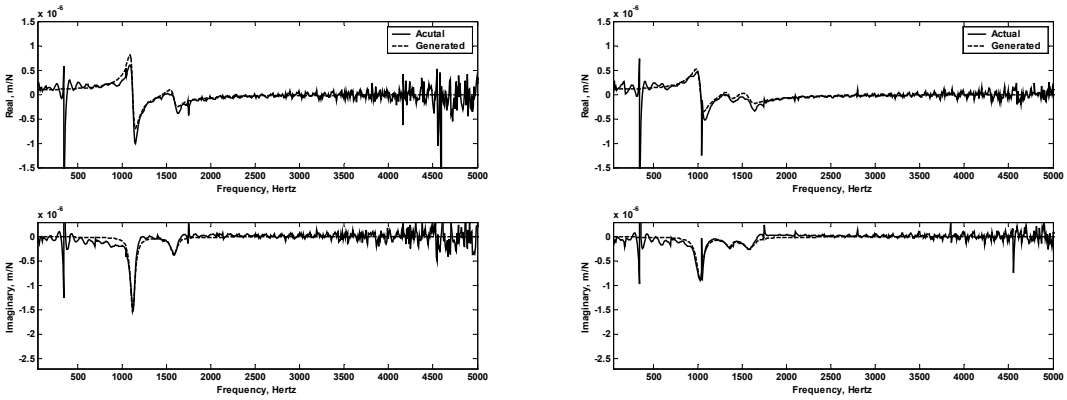

Figure D-9. FRF of the solid tool at 21000 rpm in x (left) and y (right) directions.

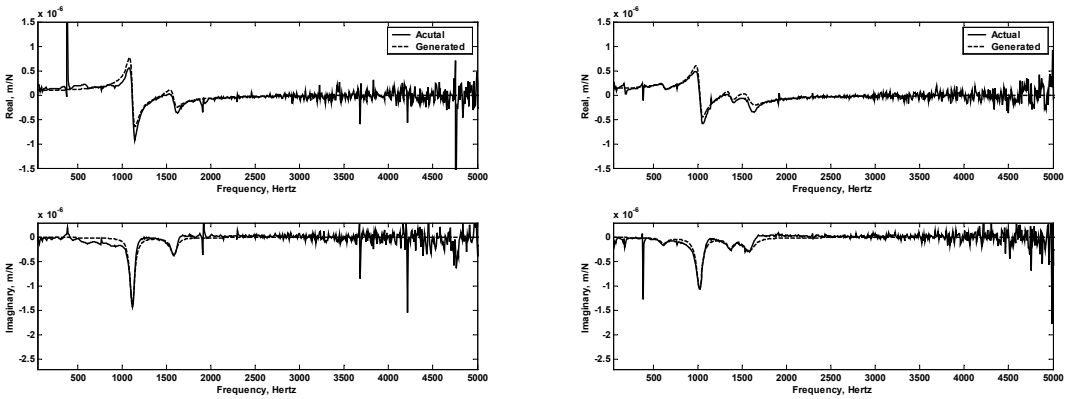

Figure D-10. FRF of the solid tool at 23000 rpm in x (left) and y (right) directions.

Hollow Tool

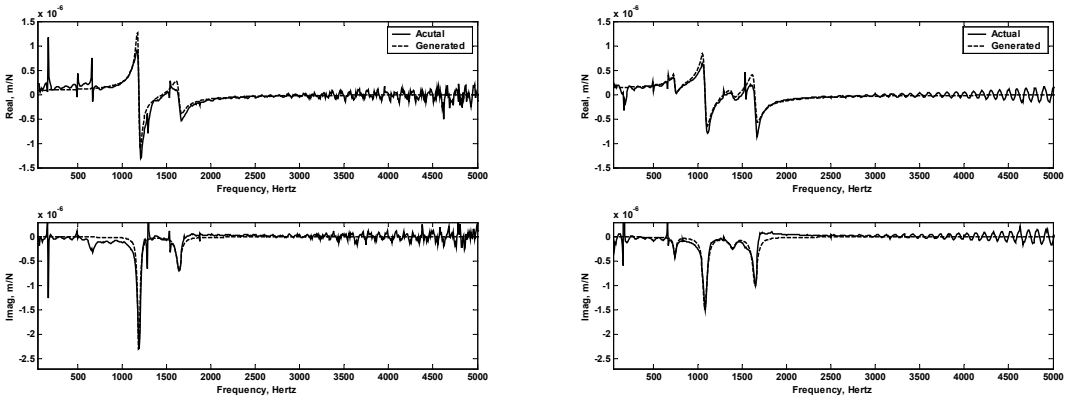

Figure D-11. FRF of the hollow tool at 10000 rpm in x (left) and y (right) directions.

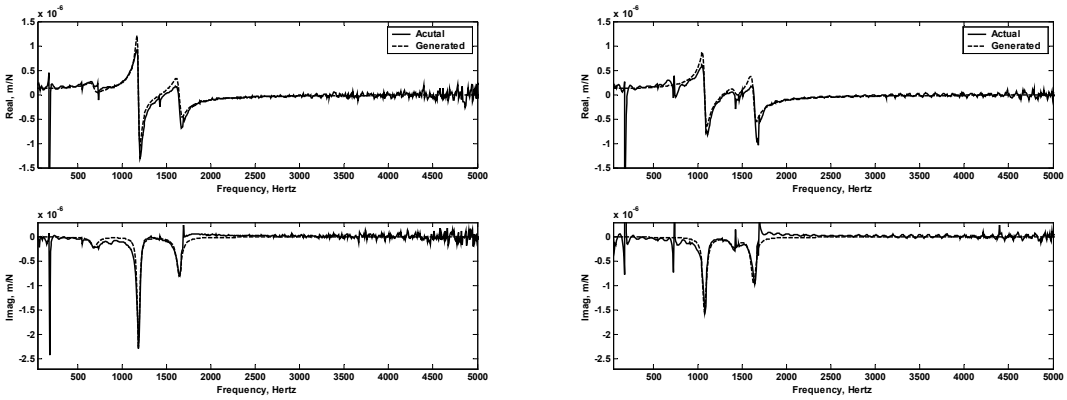

Figure D-12. FRF of the hollow tool at 11000 rpm in x (left) and y (right) directions.

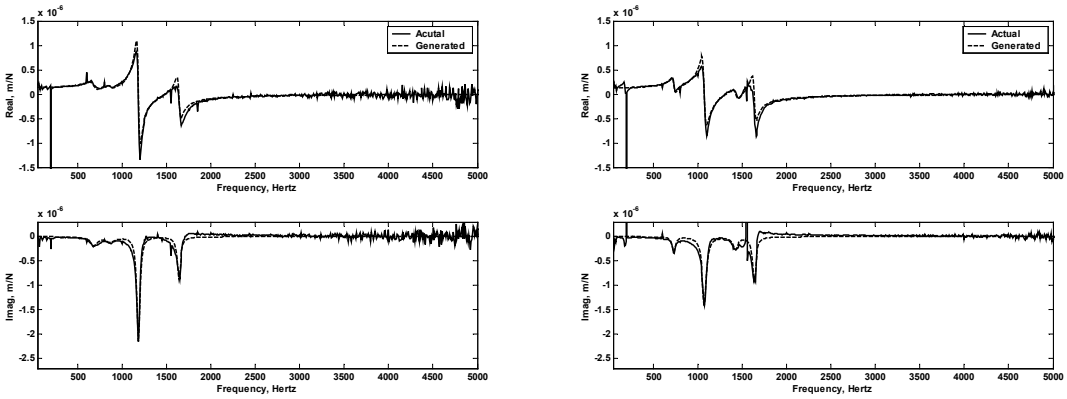

Figure D-13. FRF of the hollow tool at 12000 rpm in x (left) and y (right) directions.

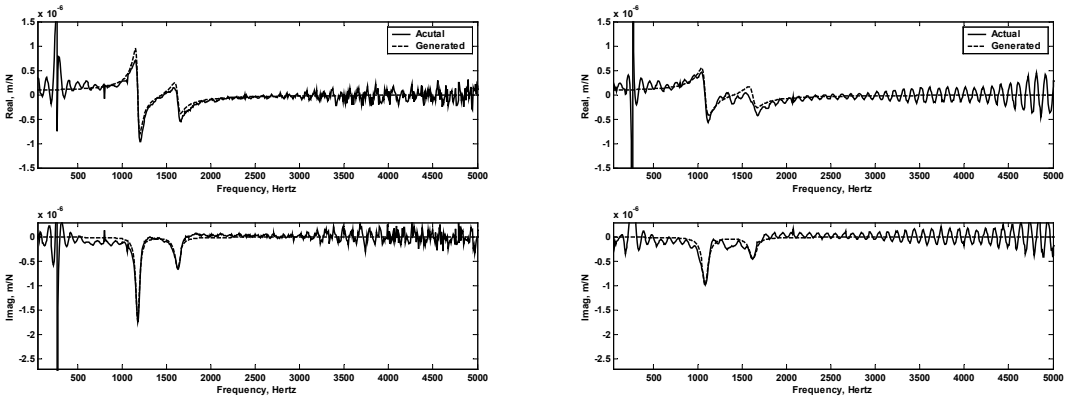

Figure D-14. FRF of the hollow tool at 16000 rpm in x (left) and y (right) directions.

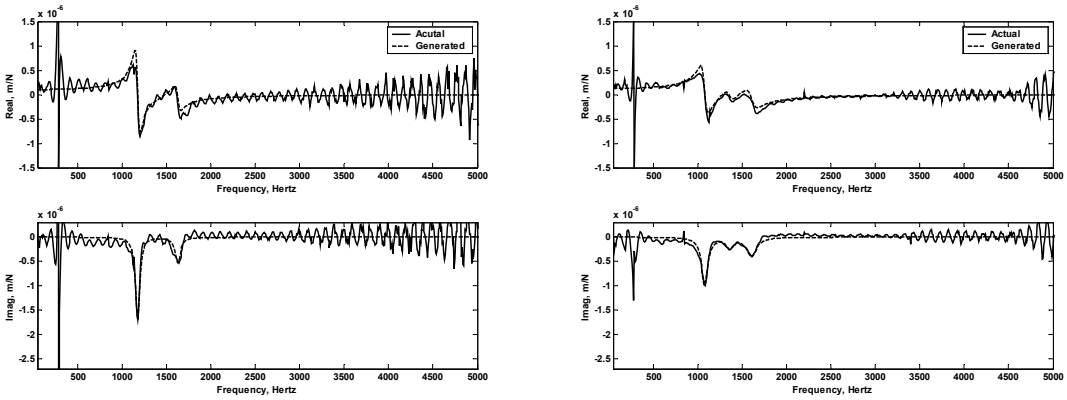

Figure D-15. FRF of the hollow tool at 17000 rpm in x (left) and y (right) directions.

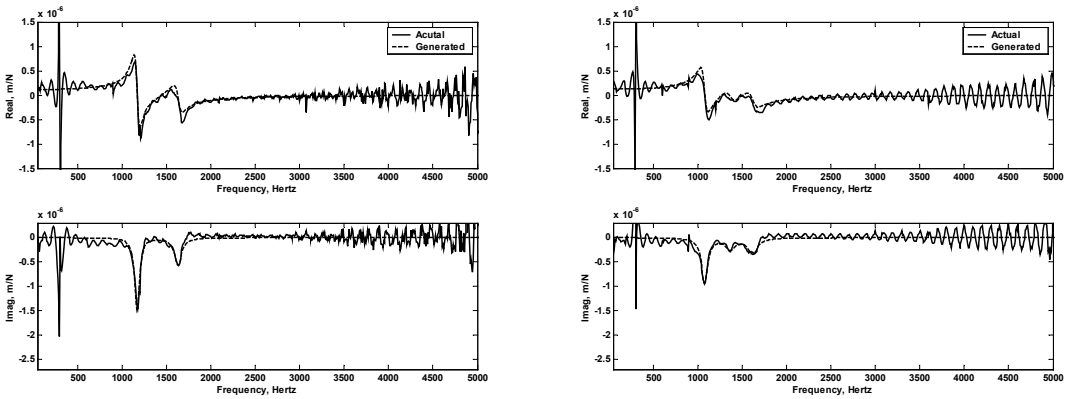

Figure D-16. FRF of the hollow tool at 18000 rpm in x (left) and y (right) directions.

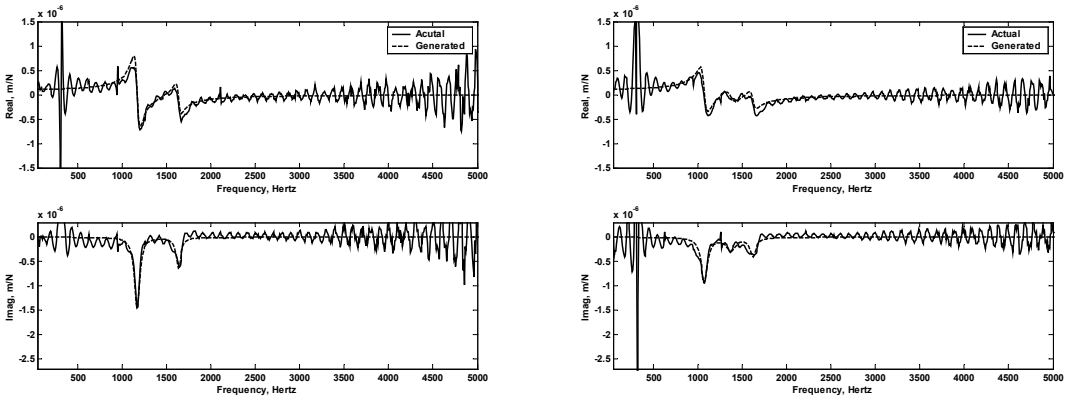

Figure D-17. FRF of the hollow tool at 19000 rpm in x (left) and y (right) directions.

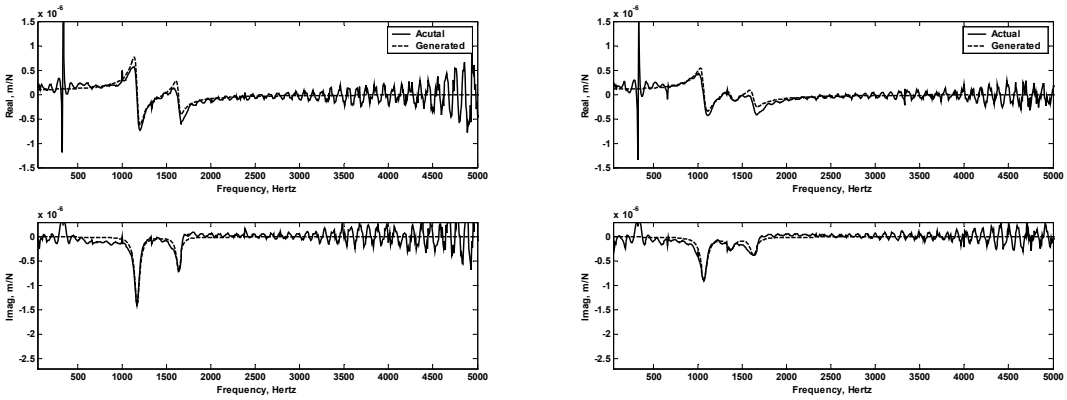

Figure D-18. FRF of the hollow tool at 20000 rpm in x (left) and y (right) directions.

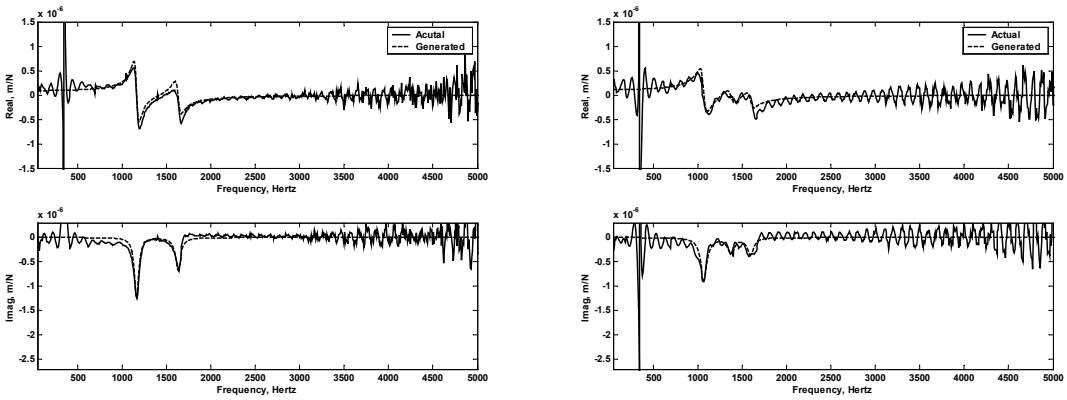

Figure D-19. FRF of the hollow tool at 21000 rpm in x (left) and y (right) directions.

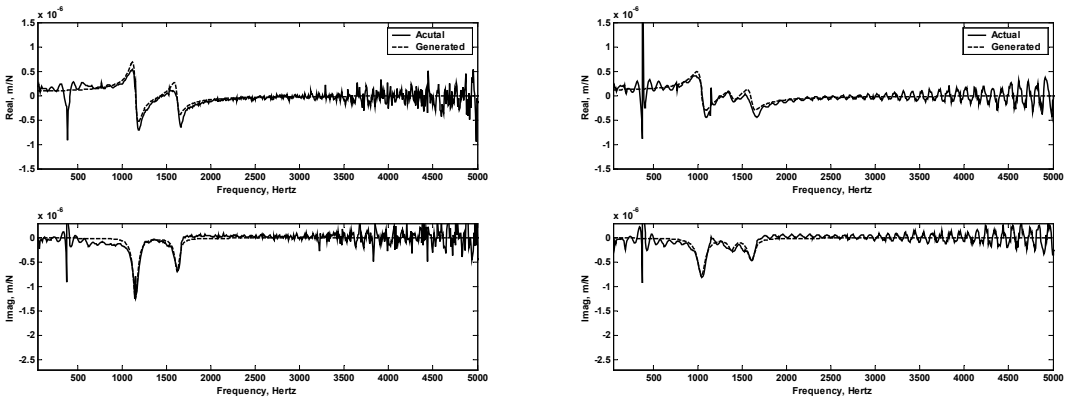

Figure D-20. FRF of the hollow tool at 23000 rpm in x (left) and y (right) directions.

Damped Tool

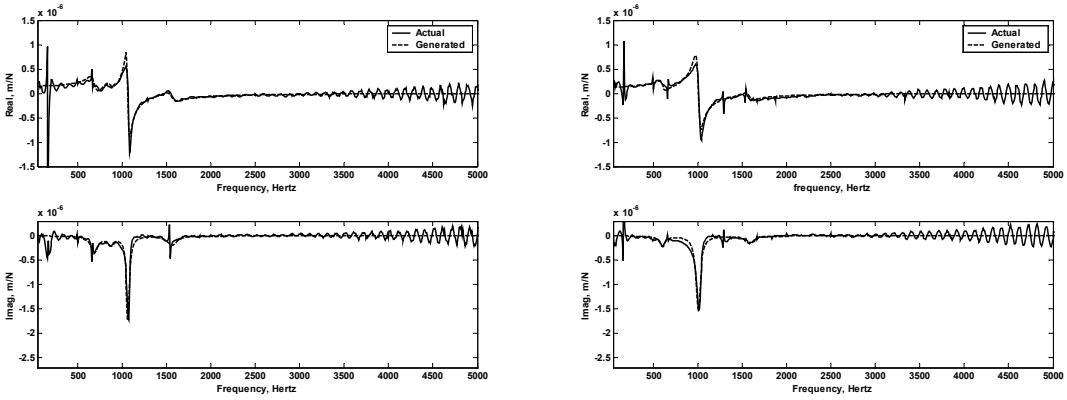

Figure D-21. FRF of the damped tool at 10000 rpm in x (left) and y (right) directions.

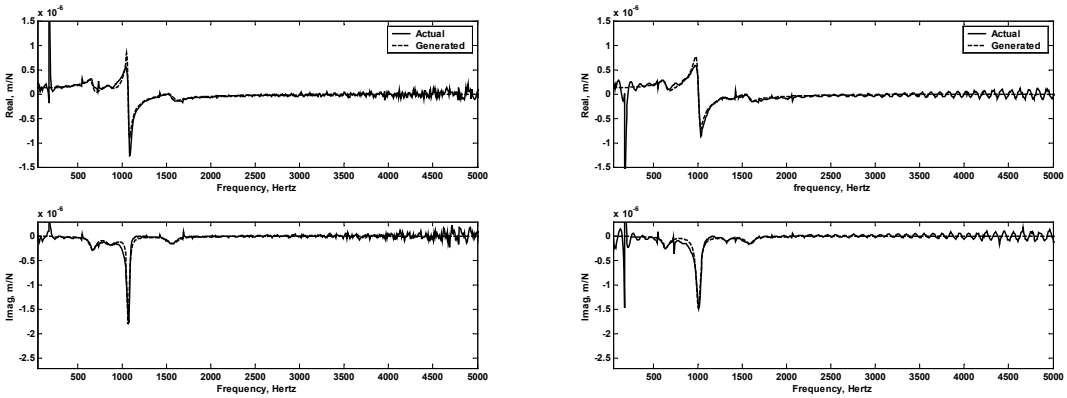

Figure D-22. FRF of the damped tool at 11000 rpm in x (left) and y (right) directions.

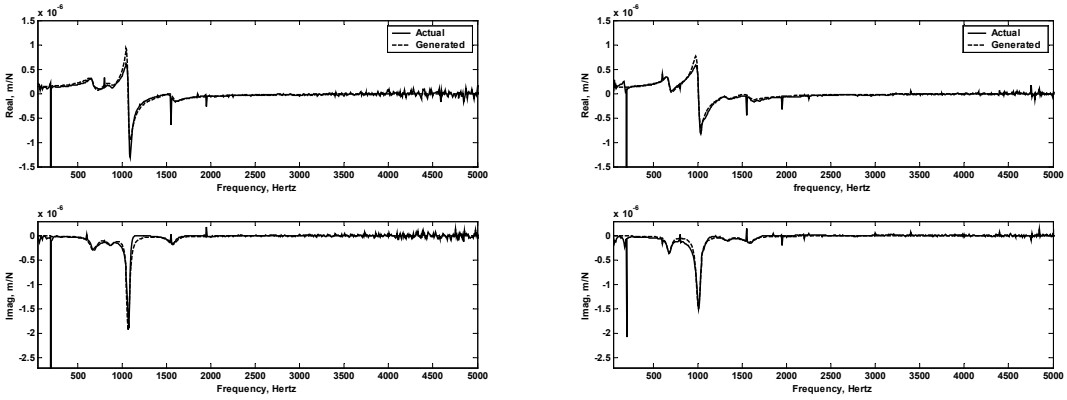

Figure D-23. FRF of the damped tool at 12000 rpm in x (left) and y (right) directions.

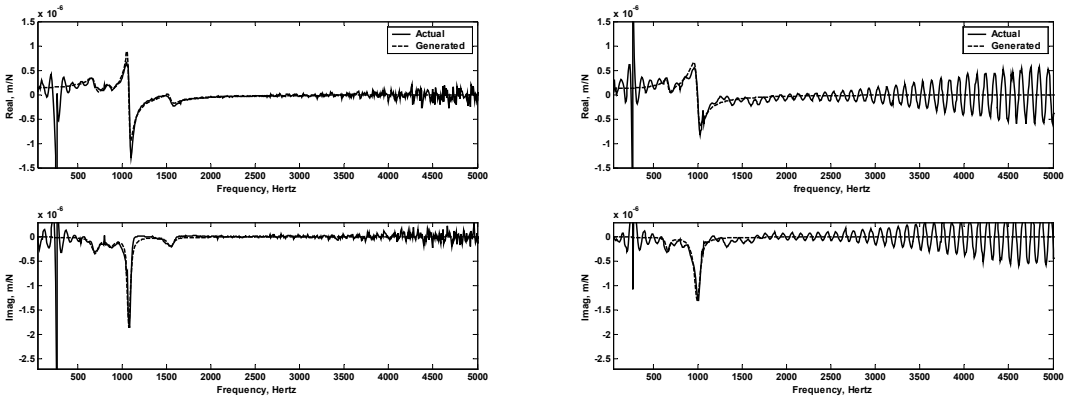

Figure D-24. FRF of the damped tool at 16000 rpm in x (left) and y (right) directions.

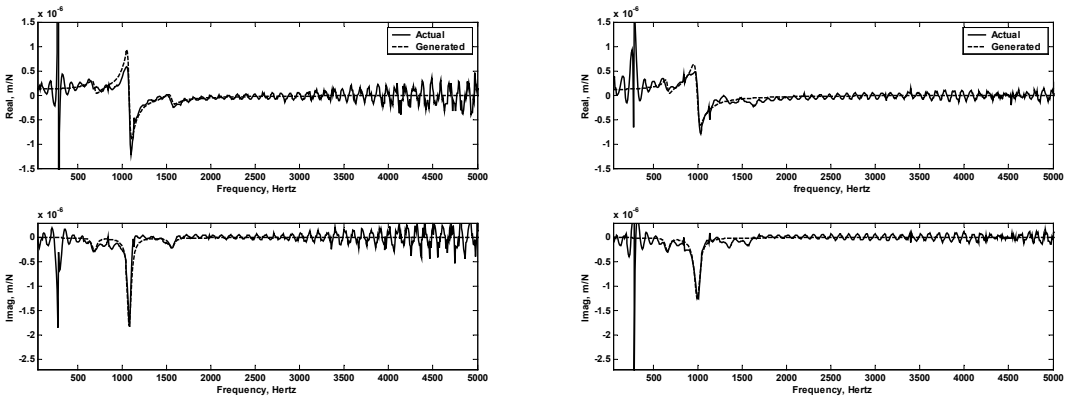

Figure D-25. FRF of the damped tool at 17000 rpm in x (left) and y (right) directions.

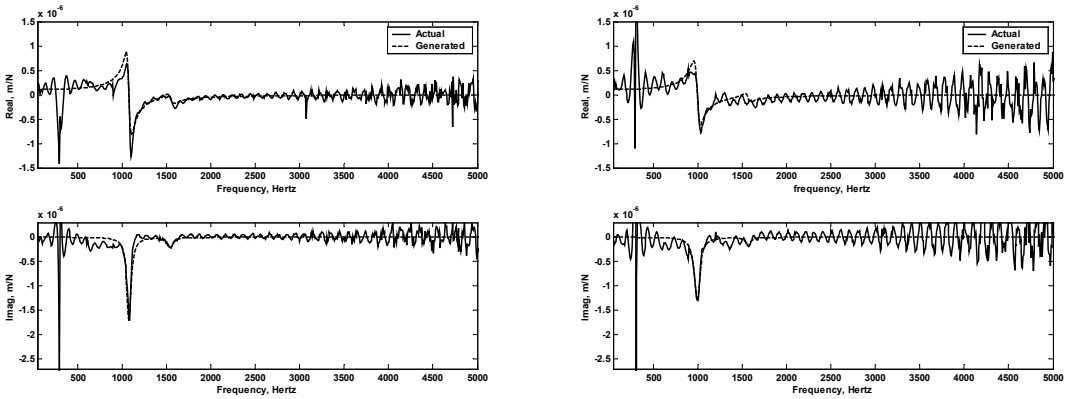

Figure D-26. FRF of the damped tool at 18000 rpm in x (left) and y (right) directions.

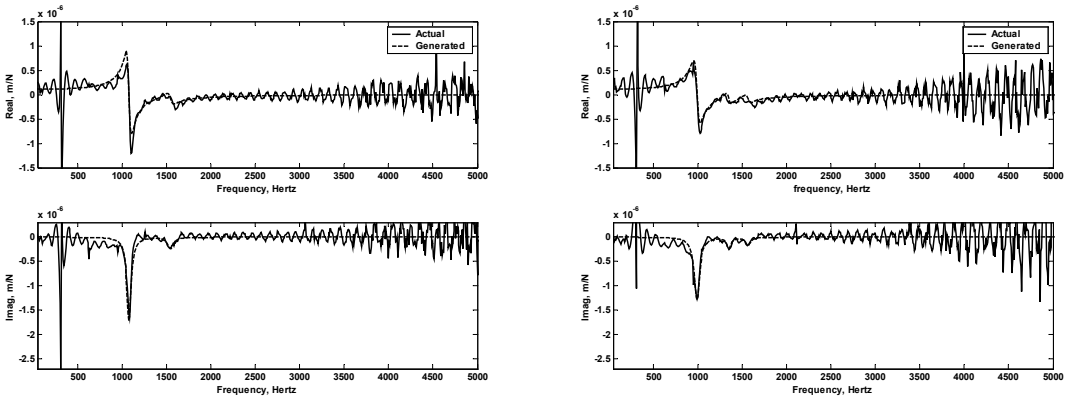

Figure D-27. FRF of the damped tool at 19000 rpm in x (left) and y (right) directions.

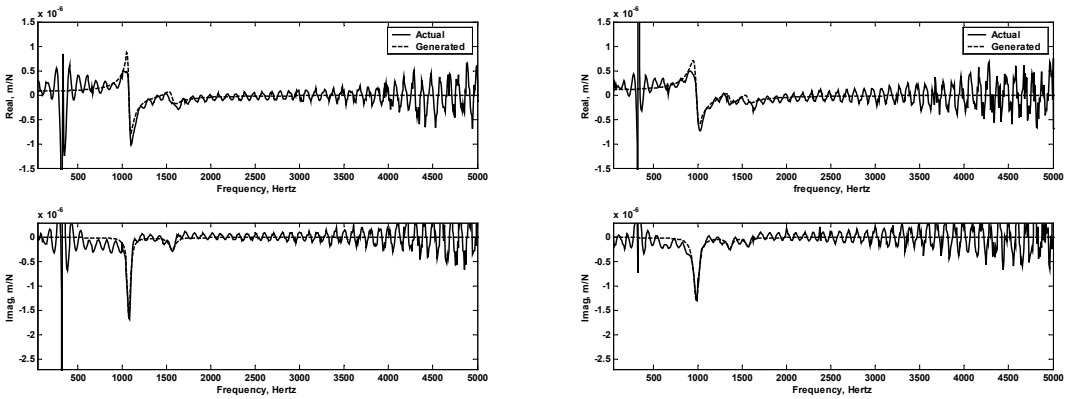

Figure D-28. FRF of the damped tool at 20000 rpm in x (left) and y (right) directions.

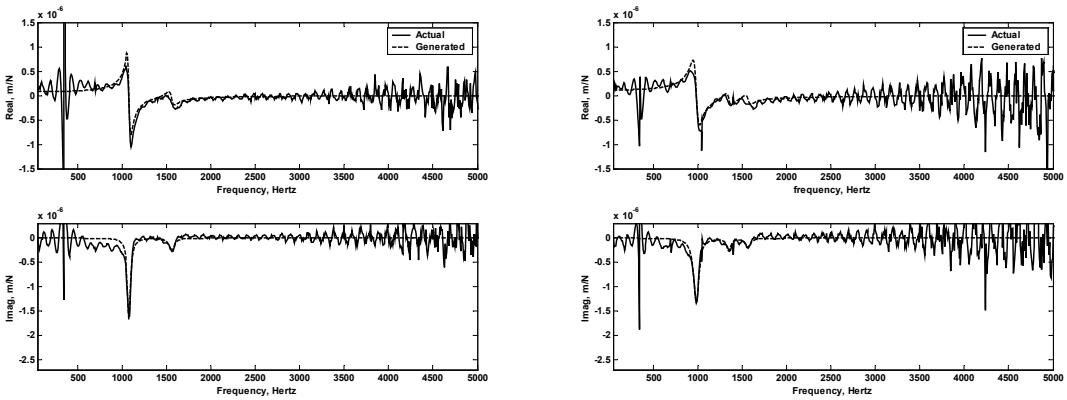

Figure D-29. FRF of the damped tool at 21000 rpm in x (left) and y (right) directions.

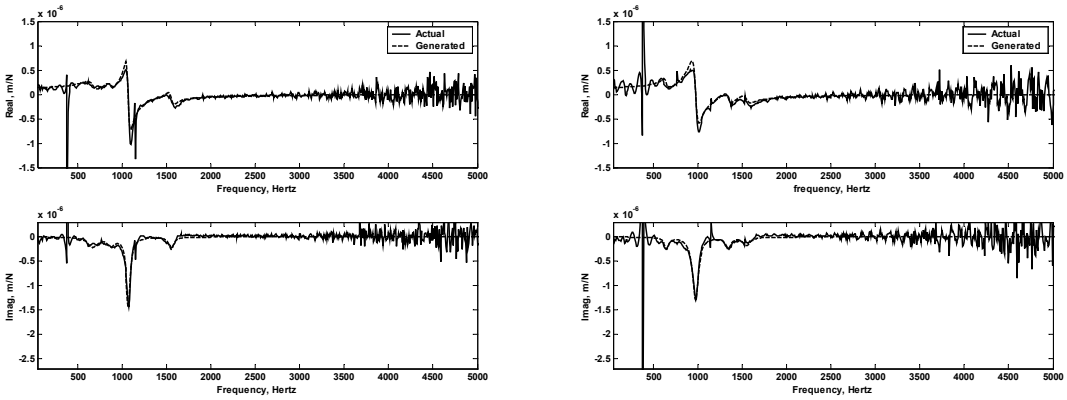

Figure D-30. FRF of the damped tool at 23000 rpm in x (left) and y (right) directions.

LIST OF REFERENCES

1. Abu-Rahmeh, Bassam, 1998, "Determination Of Machining Performance Based On Spindle Dynamics," Master's Thesis, Mechanical Engineering, University of Florida, Gainesville, FL.

2. Tlusty, George, 2000, *Manufacturing Processes And Equipment,* Prentice Hall, Upper Saddle River, NJ.

3. Edhi, Evita and Hoshi, Tetsutaro, 2001, "Stabilization Of High Frequency Chatter Vibration In Fine Boring By Friction Damper," *Precision Engineering,* Vol. 25, pp. 224-234

4. Slocum, H. Alexander, 1992, *Precision Machine Design,* Society Of Manufacturing Engineers, Dearborn, MI.

5. Schmitz, T., Donaldson, R., 2000, "Predicting High-Speed Machining Dynamics By Substructure Analysis," *Annals of the CIRP*, Vol. 49, pp. 303-308.

6. Cobb, W. T., 1989, "Design Of Dampers For Boring Bars And Spindle Extensions," Master's Thesis, Mechanical Engineering, University of Florida, Gainesville, FL.

7. Smith, Kevin Scott, 1985, "Chatter, Forced Vibrations, And Accuracy In High-Speed Milling," Master's Thesis, Mechanical Engineering, University of Florida, Gainesville, FL.

8. Keyvanmanesh, Amir, 1990, "Evaluation Of Chatter Detection And Control System," Master's Thesis, Mechanical Engineering, University of Florida, Gainesville, FL.

9. Cheng, E., 1992, "A Chatter-Free Pocketing Routine For Any Two-And-A Half-Dimensional Pocket With Islands," Master's Thesis, Mechanical Engineering, University of Florida, Gainesville, FL.

10. Cook, R. A., Bloomquist, D., Richard, D. S., and Kalajian, M.A., 2001, "Damping Of Cantilevered Traffic Signal Structures," *Journal of Structural Engineering,* Vol. 25, pp 1476-1483.

11. Slocum, H. Alexander, Concord, N. H., Marsh, R. Eric, Smith, H. Douglas, 1998, "Replicated In-Place Internal Viscous Shear Damper For Machine Structures And Components," U. S. Patent No. 5, 799, 924 (September 1, 1998).

12. Sterling, A. Robert, 2001, "Damping Of Long Endmills," Master's Thesis, Mechanical Engineering, University of Florida, Gainesville, FL.

13. Altintas, Yusuf, 2000, *Manufacturing Automation, Metal Cutting Mechanics, Machine Tool Vibrations, And CNC Design,* Cambridge University Press, Cambridge, UK.

14. Schmitz, T., in press, "Chatter Recognition By A Statistical Evaluation Of The Synchronously Sampled Audio Signal," accepted for publication in the *Journal of Sound and Vibrations*

BIOGRAPHICAL SKETCH

The author was born in November 1977 in a southern city of India now called Chennai.

He graduated from high school in May 1996 and proceeded to attend Sri Venkateswara College of Engineering, which is affiliated to the University of Madras, and earned his bachelor's degree in mechanical engineering in May 2000. In August 2000 he started graduate degree studies in mechanical and aerospace engineering at the University of Florida. He joined the Machine Tool Research Center in the same department in January 2001 and is currently working as a research assistant.